Pergamon

Geochimica et Cosmochimica Acta, Vol. 68, No. 9, pp. 2095–2118, 2004

0016-7037/04 $30.00 + .00

doi:10.1016/j.gca.2003.07.017

Anaerobic methane oxidation and a deep H_2S sink generate isotopically heavy sulfides in Black Sea sediments

Bo Barker Jørgensen,[1,*] Michael E. Böttcher,[1] Holger Lüschen,[2] Lev N. Neretin,[1] and Igor I. Volkov[3]

[1]Max Planck Institute for Marine Microbiology, Celsiusstr. 1, D-28359 Bremen, Germany
[2]Institute of Chemistry and Biology of the Marine Environment, University of Oldenburg, P.O. Box 2503, D- 26111 Oldenburg, Germany
[3]P. P. Shirshov Institute of Oceanology of the Russian Academy of Science Nakhimovskiy prosp. 36, 117851 Moscow, Russia

(*Received November* 1, 2002; *accepted in revised form July* 18, 2003)

Abstract—The main terminal processes of organic matter mineralization in anoxic Black Sea sediments underlying the sulfidic water column are sulfate reduction in the upper 2–4 m and methanogenesis below the sulfate zone. The modern marine deposits comprise a ca. 1-m-deep layer of coccolith ooze and underlying sapropel, below which sea water ions penetrate deep down into the limnic Pleistocene deposits from >9000 years BP. Sulfate reduction rates have a subsurface maximum at the SO_4^{2-}-CH_4 transition where H_2S reaches maximum concentration. Because of an excess of reactive iron in the deep limnic deposits, most of the methane-derived H_2S is drawn downward to a sulfidization front where it reacts with Fe(III) and with Fe^{2+} diffusing up from below. The H_2S-Fe^{2+} transition is marked by a black band of amorphous iron sulfide above which distinct horizons of greigite and pyrite formation occur. The pore water gradients respond dynamically to environmental changes in the Black Sea with relatively short time constants of ca. 500 yr for SO_4^{2-} and 10 yr for H_2S, whereas the FeS in the black band has taken ca. 3000 yr to accumulate. The dual diffusion interfaces of SO_4^{2-}-CH_4 and H_2S-Fe^{2+} cause the trapping of isotopically heavy iron sulfide with $\delta^{34}S = +15$ to +33‰ at the sulfidization front. A diffusion model for sulfur isotopes shows that the SO_4^{2-} diffusing downward into the SO_4^{2-}-CH_4 transition has an isotopic composition of +19‰, close to the +23‰ of H_2S diffusing upward. These isotopic compositions are, however, very different from the porewater SO_4^{2-} (+43‰) and H_2S (−15‰) at the same depth. The model explains how methane-driven sulfate reduction combined with a deep H_2S sink leads to isotopically heavy pyrite in a sediment open to diffusion. These results have general implications for the marine sulfur cycle and for the interpretation of sulfur isotopic data in modern sediments and in sedimentary rocks throughout earth's history.

1. INTRODUCTION

The Black Sea has a surface area of 423,000 km^2 and a maximal depth of 2212 m and is today the largest anoxic basin on earth (Ross and Degens, 1974). The surface water has a salinity of 17.5–18.5, whereas the deep water salinity is 22.3 (Murray et al., 1991). About 35% of the fresh water inflow comes through the Danube river which also carries half of the total sediment load from land. Much of this terrestrial material is deposited on the broad shelf and slope region of the northwestern Black Sea from where samples were taken for this study (Fig. 1; Hay et al., 1991).

During the last glaciation the Black Sea was a freshwater lake with a minimum water level at −130 m relative to present seawater level and, thus, with the modern shelf exposed as extensive coastal plains. Deep Pleistocene deposits of limnic origin are today found everywhere below 1 meter subsurface or deeper in the slope and deep sea sediments (Hay et al., 1991). Due to the melting of glaciers on the northern Eurasian continent and the postglacial rise of the global sea level, a seawater connection across the 34-m-deep sill of the Bosporus was established at least 7150 yr ago (Ryan et al., 1997; Aksu et al., 1999; Görür et al., 2001). The first evidence of seawater intrusion dates earlier, however, some 9800 yr ago (Jones and Gagnon, 1994; Arthur and Dean, 1998).

After the Bosporus connection, a stable pycnocline developed in the Black Sea between the brackish surface water, influenced by the large riverine inflow, and the more saline bottom water of Mediterranean origin. Due to the stable stratification, anoxia developed below the pycnocline, and from ~7500 yr ago an organic-rich sapropel started to accumulate, dominated by diatoms and dinoflagellates. The coccolithophorid, *Emiliania huxleyi*, invaded the Black Sea only ~3000 yr ago, and since then a varved coccolith ooze has been deposited (Calvert et al., 1987; Lyons, 1991; Hay et al., 1991; Arthur and Dean, 1998).

In the chronological description of Black Sea sediments, three depositional periods are recognized (Ross and Degens, 1974; Arthur and Dean, 1998): the modern coccolith ooze (Unit I), the marine sapropel (Unit II), and the deep limnic sediment (Unit III). Unit I has very high carbonate content, up to 65% $CaCO_3$, and relatively high organic content, ca. 4% C_{org} (Volkov, 1973; Hay, 1988). The Holocene sapropel of Unit II has a lower carbonate content of ca. 16% but is extremely rich in organic matter, 5–20% C_{org}, mostly of marine origin (Hay, 1988). The accumulation of high-organic sediments may be due to either enhanced preservation during anoxia (Brumsack, 1989; Wilkin et al., 1997; Arthur and Dean, 1998), to enhanced primary productivity during the time of sapropel formation (Calvert and Fontugne, 1987), to lower sedimentation rate of other bulk components (Calvert and Karlin, 1998), or to a combination of these factors. The limnic Unit III is very uniform, and the absence of varving shows that a bioturbating fresh water fauna was present in the oxic lake sediment.

* Author to whom correspondence should be addressed. (bjoergen@mpi-bremen.de).

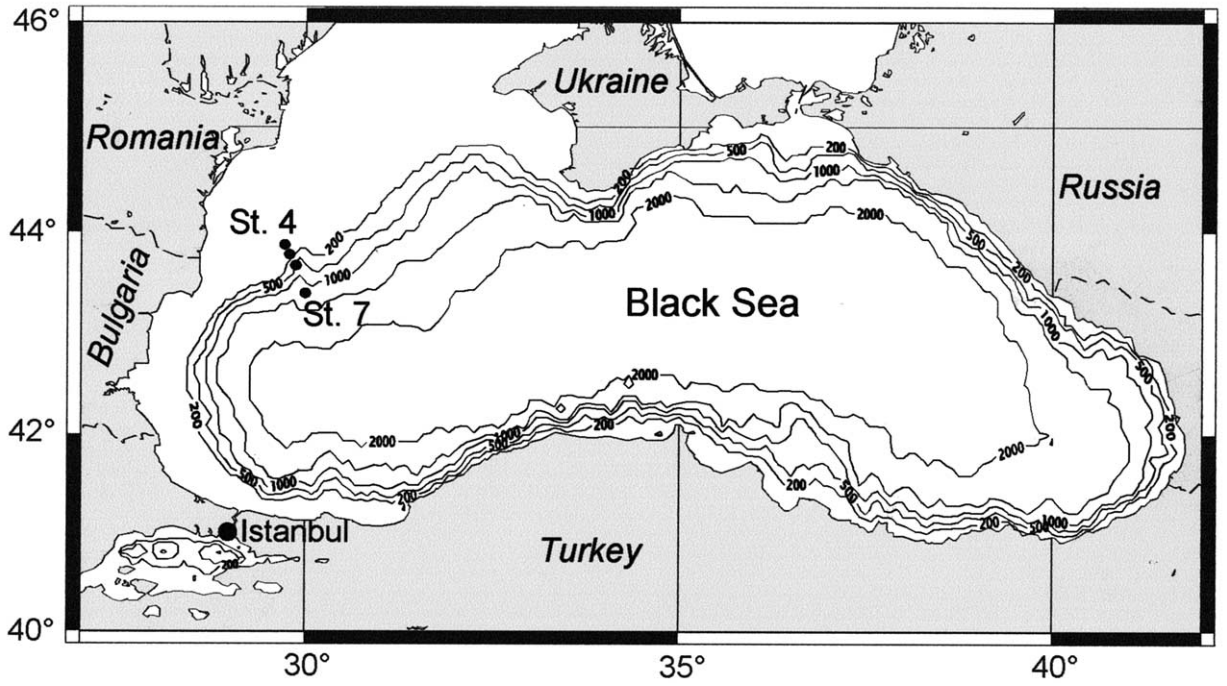

Fig. 1. Map of the Black Sea showing the positions of Stations 4 to 7 on a transect across the NW slope.

The modern Black Sea sediments below ca. 150 m water depth are overlain by a sulfidic water column, and sulfate reduction is consequently the dominant mineralization process right up to the sediment surface (Jørgensen et al., 2001). Sulfate today penetrates down through the Holocene deposits and a few meters into the limnic sediments of Unit III in which methanogenesis takes over as the terminal process of organic carbon degradation (Egorov, 2000). The methane partial pressure builds up to >1 bar at 0.5–1 m below the sulfate zone, and methane diffuses up into the transition zone where anaerobic methane oxidation drives an enhanced sulfate reduction. Methane oxidation provides the energy substrate for 7–18% of the total sulfate reduction in the sediment column and is the main source of H_2S formation at depth (Jørgensen et al., 2001).

Following the onset of seawater intrusion into the Black Sea, the high sulfate concentration has supported an enhanced production of sulfide and resulted in a progressing penetration of H_2S into the Pleistocene deposits. The sulfidization front is today visible at 2–4 m subsurface as a distinct black band in slope sediments or as many fine black layers rich in iron sulfide in the central basin (Volkov, 1961, 1984; Berner, 1974). A similar sulfidization is known to occur also in sediments of other marginal seas which were limnic during the last glaciation, e.g., the Baltic Sea (Boesen and Postma, 1988; Böttcher and Lepland, 2000). Even in pelagic marine sediments with non–steady-state deposition such sulfidization fronts may occur (Kasten et al., 1998; Pruysers, 1998).

The mechanisms and the products of this widespread sulfidization process are therefore important to understand. The reaction between downwards migrating H_2S and deeply buried iron leads initially to an amorphous iron monosulfide and subsequently to greigite, and possibly mackinawite, in the sulfidized sediment (Bonev et al., 1989). These mineral phases are metastable and are gradually converted into or replaced by pyrite, provided that sufficient sulfide and intermediate sulfur species are present (Luther, 1991; Rickard and Luther, 1997; Wang and Morse, 1996).

The pathways and mass balance of sulfur in the sediment are also reflected in the isotopic composition of the reacting and produced sulfur species. Sulfate reducing bacteria discriminate slightly against the heavy sulfur isotope, ^{34}S, and the resulting H_2S is, accordingly, enriched in the light isotope, ^{32}S. The experimentally determined fractionation factor during sulfate reduction is generally 15–30‰ in pure cultures (maximum 49‰; Bolliger et al., 2001) and up to 40‰ in sediments (Habicht and Canfield, 2001; Canfield, 2001). In the sea floor, however, the isotopic difference between sulfate and sulfide is generally larger, 40–65‰ and the resulting sulfide has been found to have an isotopic value of up to 72‰ (Böttcher et al., in press). The additional fractionation may be generated by a concurrent recycling of H_2S via an intermediate oxidation to elemental sulfur or thiosulfate by buried Fe(III) and a disproportionation of these intermediates to SO_4^{2-} and H_2S (Jørgensen, 1990; Canfield and Thamdrup, 1994; Cypionka et al., 1998; Habicht et al., 1998). The disproportionation shunts produce ^{34}S-enriched SO_4^{2-} and ^{34}S-depleted H_2S and thereby increase the resulting isotopic difference between SO_4^{2-} and H_2S in the sediment pore water.

Black Sea surface sediments have an isotopic difference, $\Delta^{34}S$, between SO_4^{2-} and H_2S of around 60‰. It has long been an enigma how this large isotope fractionation is possible in such a highly reducing environment as the Black Sea basin where reactive iron and other potential oxidants for an oxidative recycling through the disproportionation shunts would appear to be exhausted. Although a large part of the sedimenting pyrite may originate from the water column near the che-

Table 1. Station positions in the northwestern Black Sea with water depths and O_2 or H_2S concentrations in the overlying bottom water.

Station	Position	Depth (m)	O_2 (μM)	H_2S (μM)
4	43°43′08N, 030°05′90E	130	<5	0
5	43°42′63N, 030°06′12E	181	0	8
6	43°40′47N, 030°07′54E	396	0	75
7	43°31′61N, 030°13′33E	1176	0	295

mocline and is thereby deposited with a strongly ^{34}S-depleted signal (Muramoto et al., 1991), also the SO_4^{2-} and H_2S in the sulfidic bottom water have this large isotopic difference between $\delta^{34}S$ values of ca. +20‰ in SO_4^{2-} and −40‰ in H_2S (Fry et al., 1991; Neretin et al., 1998b).

In the deep limnic deposits the $\delta^{34}S$ of pyrite increases steeply with depth up to ca. +20‰ (Vinogradov et al., 1962; Calvert et al., 1996). The sulfur isotopic composition of iron sulfide, elemental sulfur, and pyrite at the sulfidization front may even reach values as high as +25 to +38‰ (Lie, 1994; Nicolaev, 1995). The formation of extremely heavy pyrite was explained as a result of: A) very high sulfate reduction rates at the time of deposition, whereby the isotopic fractionation was negligible and the $\delta^{34}S$ of H_2S would be close to the +20‰ of seawater SO_4^{2-}; or B) closed system conditions, by which the pyrite was formed from a ^{34}S-enriched sulfate pool (Vinogradov et al., 1962; Calvert et al., 1996).

The present paper concludes a very different mechanism of heavy sulfide formation. Our study was undertaken to better understand the geochemistry and dynamics of sulfur cycling in the deep Black Sea sediments, especially of the sulfidization front in the limnic part. We wanted to explain the shift from isotopically very light sulfides near the surface to extremely ^{34}S-enriched sulfur below the sapropel. The results will show that interactions with methane and iron diffusing up through the Pleistocene deposits provide the key to the formation of heavy sulfides and that the mechanisms involved are probably operating widely in marine sediments.

2. MATERIAL AND METHODS

2.1. Sampling

Sediment cores were taken during a research cruise of the Russian *R/V Petr Kottsov* in the western Black Sea in September 1997. Four stations were sampled from the Romanian shelf break and into the western basin at water depths ranging from 130 to 1176 m (Fig. 1; Table 1). The two shallower stations were situated just above and just below the depth where the oxic–anoxic interface of the water column impinged on the sea floor at 140–150 m depth. The two other stations were situated deep within the sulfidic zone. At each station, 1–2 cores of 5–8 m length and 12 cm I.D. were taken by gravity corer and a set of 40–50 cm deep and 10 cm I.D. surface cores were taken by multicorer. Care was taken to return to the same satellite position for repeated sampling. For each station, all data are derived from a single gravity core. Accurate depth alignment of gravity cores and multicores was done by comparing sapropel depths and from characteristic pore water and solid-phase gradients. In this paper, mostly results from the gravity cores will be presented. Concurrent studies of the biogeochemistry and microbiology in the surface sediments are described elsewhere (Roselló-Mora et al., 1999; Thamdrup et al., 2000; Weber et al., 2001; Wenzhöfer et al., 2002).

A hydrocast and a Conductivity-Temperature-Depth (CTD) profile were taken at each station. The temperature of the bottom water increased with water depth from 8.6°C at Station 4 to 9.1°C at Station 7.

2.2. Pore Water Analyses

Subcores of 36 mm I.D. were taken in acrylic coring tubes from the multicores and were subsequently sectioned for analyses of pore water and solid-phase chemistry. Gravity cores were kept nearly horizontal on the deck in 3–5 m lengths within the core liners and, within a few hours after retrieval, were pushed out stepwise at the upper core end by a large piston. This procedure was adapted to minimize loss of dissolved gases (CH_4 and H_2S) or oxidation of redox-sensitive solutes such as Fe^{2+}. For each 10 or 20 cm, the piston was stopped, the core end was cut clean, and a set of subsamples was immediately taken from the central part of the core by syringes with cut-off ends. Different samples were used for pore water and solid-phase analyses. Further details of this sampling procedure are given in Jørgensen et al. (2001).

Pore water was squeezed, within 30 min after sampling, through 0.45-μm cellulose acetate membrane filters under 3–5 bar N_2 pressure. The pore water was led directly into dilute $ZnCl_2$ to fix H_2S as ZnS. Sulfide was measured by the photometric methylene blue method (Cline, 1969) after appropriate dilution of the $ZnCl_2$-preserved samples. (The total dissolved sulfide is in this paper called sulfide or H_2S; when the dissolved, nondissociated or dissociated form is specifically meant, these are written in italics: H_2S or HS^-). Dissolved ferrous iron was measured by inductively coupled plasma optical emission spectroscopy (Perkin Elmer Optima 3000 XL). A minor blank contribution from the added zinc chloride was subtracted. Sulfate was analyzed by nonsuppressed ion chromatography and methane by gas chromatography using a flame ionization detector and a Porapak-Q 80/100 column as described by Jørgensen et al. (2001).

2.3. Solid-phase Analyses

Total carbon (TC) was measured on freeze-dried samples using a LECO SC-444 instrument. Total inorganic carbon (TIC) was measured on a CM 5012 CO_2 coulomat with a CM5140 acidification device. The TIC was recalculated to the equivalent amount of $CaCO_3$ (although other carbonates also may be present). TOC contents were obtained from the difference between TC and TIC.

Sediment samples used for determination of acid volatile sulfur (AVS = H_2S + FeS + partly Fe_3S_4) and chromium reducible sulfur (CRS = FeS_2, S° and remaining part of Fe_3S_4) were preserved in 1:1 (v/v) of 20% ZnAcetate (w/v). Subsamples of 0.5 g were treated with the two-step acid Cr(II) method (Fossing and Jørgensen, 1989) and the trapped sulfide from each step (AVS and CRS) was analyzed upon dilution by the methylene blue method (Cline, 1969). This method does not allow a clear separation of greigite, Fe_3S_4, among the two fractions. Greigite dissolves in the first step in hot HCl but

disintegrates to mostly H_2S and S°, of which the S° is included in the second step. The greigite distribution may be ca. 2/3 in the AVS fraction and 1/3 in the CRS fraction (cf. Cornwell and Morse, 1987). Elemental sulfur was extracted by acetone and then reduced by 1M $CrCl_2$ in 3N HCl under a continuous flow of argon for 30 min at room temperature (Zhabina and Volkov, 1978). The evolved H_2S was trapped in ZnAcetate and analyzed by the methylene blue method (Cline, 1969). Organic sulfur was determined after the other extractions by complete oxidation to sulfate by hot HNO_3 and $KMnO_4$ treatment, followed by hot Br_2-HNO_3. The sulfate was reduced to sulfide using Kiba Sn(II)-H_3PO_4 reagent (Volkov and Zhabina, 1980) and analyzed by the methylene blue method (Cline, 1969).

Iron in FeS and FeS_2 was determined following the two-step Cr(II) extraction described above. Reactive Fe(II) and Fe(III) were subsequently determined after extraction by 3.5 N H_2SO_4 for 4 h at room temperature under a CO_2 gas phase (Sokolov, 1980). For the determination of Fe(II) by the dichromate method, a 25-mL aliquot was mixed with 15 mL of Knopp solution (150 mL conc H_2SO_4 + 150 mL conc H_3PO_4 in 1 L) and titrated with 0.02 N $K_2Cr_2O_7$ using 0.5% sodium diphenylaminsulfonate as an indicator. For the determination of Fe(III) by iodine titration, 5 mL 1 N HCl and 3 g KJ were added. After 20 min in the dark, the solution was titrated by 0.02 N $Na_2S_2O_3$ using starch as an indicator.

The chemical data and process rates will be reported mostly in molar units per sediment volume to facilitate recalculations from concentration to vertical fluxes and areal pool sizes.

2.4. Stable Sulfur Isotopes

Sulfur isotope ratios, $^{34}S/^{32}S$, were measured by combustion isotope ratio mass spectrometry. Subsamples for $\delta^{34}S$ were taken from the same pore water samples as the subsamples for analyses of SO_4^{2-} and H_2S concentrations. Sulfide from pore water samples and AVS and CRS from the two-step Cr(II) reduction were converted into silver sulfide precipitate. Sulfate from pore water samples was trapped as barium sulfate. The cleaned and dried precipitates were combusted in a Carlo Erba EA1108 Elemental Analyzer coupled to a Finnigan MAT 252 mass spectrometer via a Finnigan MAT Conflo II split interface (Böttcher et al., 2000). Isotope ratios are reported in the δ-notation ($\delta^{34}S$) with respect to SO_2-based Vienna Canyon Diablo Troilite (V-CDT; Beaudoin et al., 1994) standard: $\delta^{34}S = [(R_{sample}/R_{V\text{-}CDT}) - -1] \times 1000‰$, where $R = {}^{34}S/{}^{32}S$. Replicates of sulfur isotopic analyses agreed within ±0.2‰. International silver sulfide standards, IAEA-S-1 with $\delta^{34}S = -0.30‰$ and IAEA-S-2 with $\delta^{34}S = +21.54‰$, were used for calibration of the mass spectrometer.

2.5. Other Determinations

Porosities were determined at 2–5 cm depth intervals in multicores and 20–40 cm depth intervals in gravity cores. The porosities were calculated from weight-volume determinations followed by drying at 105°C until constant weight and then reweighing. These data were also used to recalculate solid-phase constituents from units of sediment dry weight to units of sediment volume.

2.6. Flux and Turn-over Calculations

Pore water profiles of sulfide were used to calculate rates of net sulfide production or consumption by one-dimensional numerical modeling. We applied the modeling software, PROFILE, of Berg et al. (1998), which first divides the sediment into an arbitrary number of equidistant zones, each with a constant process rate, and provides an objective selection of the simplest process rate distribution that optimally reproduces the measured concentration profile. The criterion for optimal fit is to minimize the sum of squared deviations (SSE) from the data for each zone with different numbers of equally spaced zones. The model provides F tests for different fits and suggests the minimum number of zones that provide an optimal fit. The model ensures continuity of fluxes between zones and thus provides also fluxes of the solutes.

Boundary conditions were: zero H_2S concentration and zero H_2S flux at the bottom of the H_2S zone. Given the fast turn-over of H_2S (see below), we assumed that the concentration profiles represent steady state and that vertical transport took place by molecular diffusion only. Due to the absence of macrofauna in the anoxic Black Sea, bioirrigation can be excluded. Process rates were calculated in volume units of sediment per day (nmol cm^{-3} d^{-1}). From the volumetric rates in defined depth intervals, the areal rates under a square meter of sea floor were calculated for that interval in units of mmol m^{-2} d^{-1}.

Rate and flux data for concurrent sulfate reduction and methane oxidation in the same sediment cores were taken from Jørgensen et al. (2001).

Diffusion coefficients (D) for pore water H_2S and Fe^{2+} were taken from Schulz (2000). For sulfide we assumed a mean sediment pH of 7.5 (values measured directly in the H_2S zone during *R/V METEOR* Cruise M51/4 were 7.1–7.9; M. E. Böttcher, unpublished data). The dissociation distribution between the two species, H_2S and HS^-, was thus 1:4. The diffusion coefficient for SO_4^{2-} was taken from Iversen and Jørgensen (1993). All diffusion coefficients were recalculated to the in situ temperature of 9°C and were: for $H_2S = 1.30\ 10^{-5}$ and for $HS^- = 1.20\ 10^{-5}$ cm^2 s^{-1}, yielding an effective diffusion coefficient for H_2S ($H_2S + HS^-$) = $1.22\ 10^{-5}$ cm^2 s^{-1}; for $Fe^{2+} = 0.43\ 10^{-5}$ cm^2 s^{-1}; for $SO_4^{2-} = 0.66\ 10^{-5}$ cm^2 s^{-1}.

Sediment diffusion coefficients (D_s) were calculated using the measured porosities (φ) and the empirical equation of Iversen and Jørgensen (1993):

$$D_s = D/(1 + 3(1 - \varphi)). \quad (1)$$

Vertical diffusion fluxes (J) of pore water solutes were calculated according to:

$$J = -D_s\varphi(dC/dz) \quad (2)$$

where C is the solute concentration in the pore water and z is the depth below the sediment surface.

2.7. Definitions and Database

Different approaches were applied to identify and quantify processes. Sulfate reduction was measured experimentally by the use of ^{35}S-labeled sulfate (*gross sulfate reduction*), or was modeled from the pore water gradients of dissolved sulfate (*net sulfate reduction*). Because sulfate reduction leads quantita-

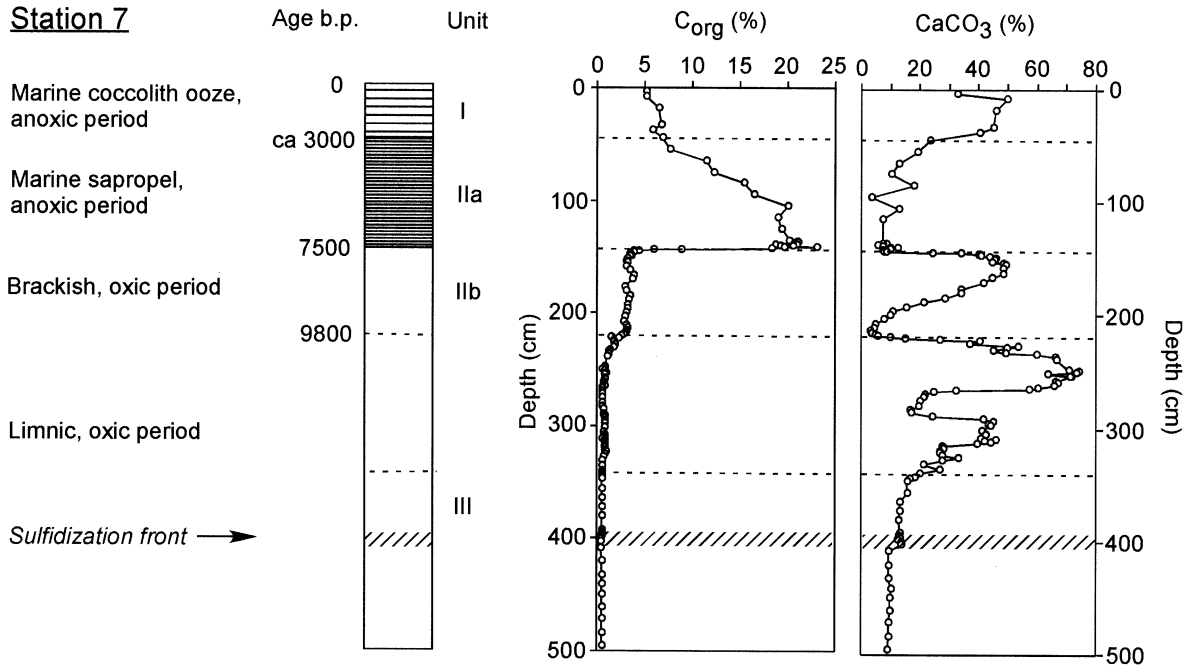

Fig. 2. Station 7 at 1176 m water depth. The main stratigraphic sequences are indicated and related to the distribution of organic carbon and carbonate (both as percent of the total dry weight of the sediment).

tively to H_2S, also the *net H_2S production* based on modeling of pore water H_2S gradients is a measure of sulfate reduction. It should be noted that there are important differences between these rates, which will be evident from the present Black Sea data:

A) The directly measured *gross sulfate reduction* rate comes closest to the total rate of sulfate reduction in the sediment. The ^{35}S method is not free of artifacts, such as rapid reoxidation of H_2S near the sediment surface during incubation, but such artifacts should be insignificant in the highly reducing and sulfidic Black Sea sediments.

B) The modeled *net sulfate reduction* rate represents the gross sulfate reduction rate minus the (long-term) rate of reoxidation of reduced sulfur species back to sulfate within the modeled depth interval.

C) The modeled *net H_2S production* rate is a measure of the gross sulfate reduction minus the reoxidation of sulfide and minus the H_2S loss by precipitation of metal sulfides or sulfidization of organic matter within the modeled depth interval.

All data presented graphically in this paper will become available in the international geoscience database, PANGAEA, and can be accessed via the internet (www.pangaea.de).

3. RESULTS

3.1. Sediment Stratigraphy

The stratigraphic record of the Black Sea sediments is best preserved at the deep stations where anoxic conditions have prevented bioturbation over the last 7500 yr and have left finely laminated deposits. Station 7, which will be described first because it has the most pronounced stratigraphy, was situated at the lower part of the slope and was clearly affected by several turbidites in the past. Station 6 at the top of the slope, yet still in the sulfidic region, apparently had a continuous sedimentation record unaffected by turbidites. The shallower stations at the shelf break showed indications of anoxic deposition in the upper 20–30 cm but did not have an undisturbed sedimentation.

Station 7 (1176 m, Fig. 2). A 3-cm-thick layer of grayish fluff covered the more consolidated sediment. The surface deposit was a very soft, grayish-brown, finely laminated coccolith ooze with an organic carbon content of 5–7%, which is within the range of sapropelic sediments. The TIC corresponded to 40–50% $CaCO_3$, which is at the high end for modern Black Sea sediments (Müller and Stoffers, 1974). This ca. 50-cm-thick Unit I layer changed gradually into a darker brown to olive sapropel which below 100 cm had ca. 20% C_{org} and 10% $CaCO_3$. The sapropel had an elastic texture and was homogeneous and finely laminated but without the fine white bands of coccoliths found in Unit I. The Unit IIa-IIb transition was very sharp, from almost black sapropel to gray clay without lamination, and marks the onset of anoxia in the deep Black Sea ~7500 yr ago. The organic carbon content dropped from 18% to 6% over an interval of only 1.5 cm at 145 cm depth. Coccoliths originating from *Emiliania huxleyi* were found by scanning electron microscopy down to 153 cm depth, i.e., 8 cm deeper than the sapropel (Lüschen, 1998). This probably marks the time when the salinity of the upper water column had reached 11, which is the minimum required for the growth of this plankton species (Bukry, 1974).

The underlying Unit IIb may represent a period when Mediterranean seawater had started to enter the Black Sea ~9800 yr

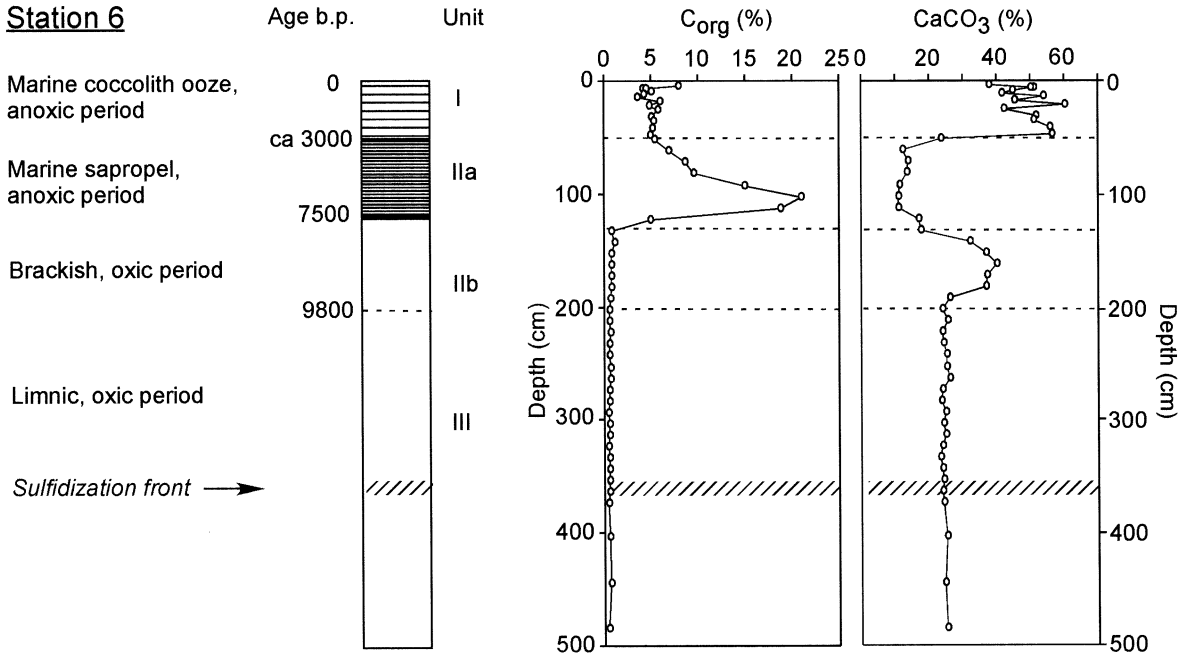

Fig. 3. Station 6 at 396 m water depth. The main stratigraphic sequences are indicated and related to the distribution of organic carbon and carbonate.

ago. The transition between IIb and III is set at 215 cm but could potentially be at 340 cm and still requires confirmation by more accurate dating. The enhanced organic deposition may indicate that this inflow was bringing nutrient-rich deep water up into the photic zone and stimulating the primary productivity. Thus, in Unit IIb the organic carbon content was much higher, 3–4%, than it had been during the earlier limnic period. The organic carbon and, in particular, the $CaCO_3$ content increased up through the limnic period. The upper limnic layer (215–340 cm) had only slightly elevated organic carbon content of 0.8% relative to the underlying limnic deposit with 0.5% C_{org}. The upper part of Unit III was characterized by highly varying (2–72%) carbonate content and was probably affected by turbidites during the latest limnic period. Highly resolved depth profiles of solid-phase trace elements normalized to aluminum (e.g., Zr/Al, Si/Al, and Ti/Al) support the occurrence of turbidites in Unit III above 400 cm depth but indicated no turbidites in Unit II or I (Lüschen, 1998). The limnic deposits generally have $CaCO_3$ concentrations of 10–40% (Müller and Stoffers, 1974). The 400 cm depth marks a modern sulfidization front caused by a progressing marine diagenetic alteration with precipitation of authigenic carbonate and of iron sulfide due to downward diffusion of H_2S. From ~400 cm and deeper, the limnic sediment was diagenetically unaltered. Below 450 cm the color was light brown. The recovered sediment core from below 400 cm had fine cracks due to overpressure of dissolved methane gas.

Calvert and Fontugne (1987) and Arthur and Dean (1998) found that the deep limnic deposits mostly consist of terrestrial material. Scanning electron microscopy of the abundant $CaCO_3$ in Unit II and III of the present cores showed authigenic and strongly weathered carbonates (Lüschen, 1998). The high terrestrial input during the limnic stage resulted in high sedimentation rates of perhaps 0.6 mm yr^{-1} (Lüschen, 1998). The sharp onset of sapropel formation at ≤145 cm depth can be used to calculate an average sediment accumulation rate for the last 7500 yr of the anoxic marine period: 0.19 mm yr^{-1}. This is close to the estimate by Jones and Gagnon (1994) of 0.2 mm yr^{-1} for Unit I+II. According to Calvert and Karlin (1998) and Hay (1988), Unit I had about twice as high sedimentation rate as Unit II. However, the Unit I/II transition is not sharp in this core and its dating therefore not accurate.

Station 6 (396 m, Fig. 3). Relative to Station 7, the sediment of Station 6 had a more uniform stratigraphy. Down to 50 cm the laminated coccolith ooze had an organic carbon content of 5% and a carbonate concentration exceeding 50% just below the 2-cm-thick fluffy surface layer. The underlying sapropel (Unit IIa), which had a peak organic carbon content of 20%, ended at 130 cm depth. At 120–140 cm depth the sediment was light-gray and had distinct lamination with fine white bands of carbonate similar to the coccolith ooze at the surface. Again, the onset of coccolith deposition at 140 cm depth presumably marks the time when the salinity had reached 11. The brackish to limnic sediment below had a uniformly low organic carbon concentration decreasing with depth from 0.8% (Unit IIb) to 0.5% (Unit III). Microscopy of preserved diatom frustrules showed limnic species up to the IIb/III transition (A. Kohly, personal communication). Based on the Unit IIa/IIb transition, a mean sedimentation rate of 0.17 mm yr^{-1} was calculated for the entire anoxic marine period.

Station 5 (181 m, Fig. 4). This station had a rather heterogeneous surface sediment which in most multi-cores was finely varved down to 20–30 cm. Here, just below the shelf break, the sediment was apparently influenced by sediment transport from the shelf caused by the strong peripheral cyclonal current in the western Black Sea. There were many shells of the fresh water

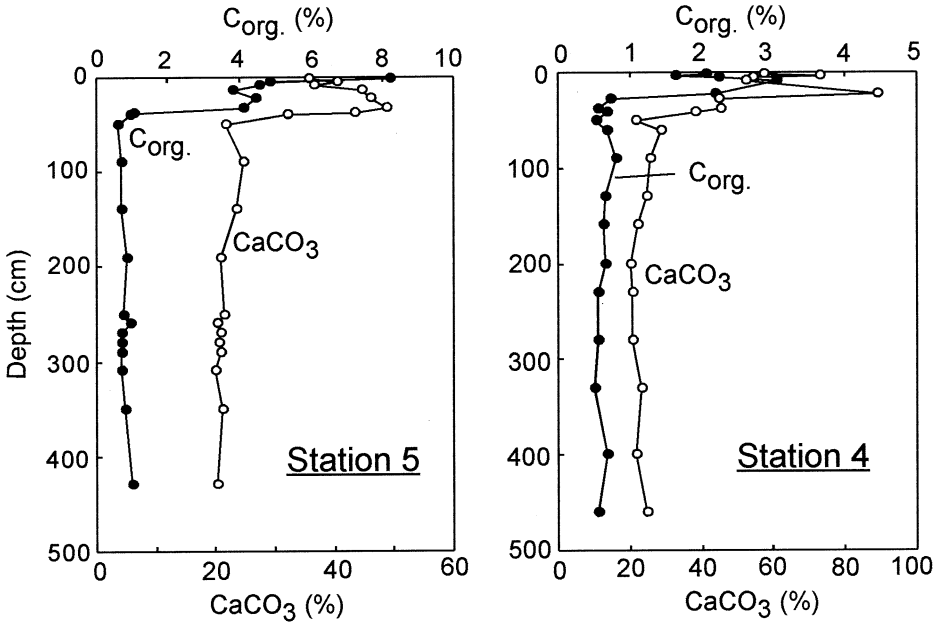

Fig. 4. Station 5 at 180 m and Station 4 at 130 m water depth. These stations are located just below and above the modern oxic–anoxic interface, respectively. At Station 5, the 35-cm-deep sapropel can be clearly recognized, whereas at Station 4 the upper layers are more disturbed.

bivalve, *Dreissena*, in the upper 30–40 cm. This indicates that, further up on the shelf, sediment erosion had exposed former limnic deposits with subsequent transport of the shells. The carbonate and organic carbon contents were high down to 35 cm depth, below which they dropped to low and constant values. Thus, the marine sapropel-like sediment started from the sediment surface, and the shift at 35 cm depth probably represents the Unit II/III transition.

Station 4 (130 m, Fig. 4). The surface sediment had no living macrofauna due to the very low oxygen concentration of the bottom water (<5 μM O_2; Table 1) but only nematodes and other meio- and microfauna (Wenzhöfer et al., 2002). Empty shells of the mussel *Modiolus phaseolinus* were abundant at the surface, which partly explains the high and fluctuating $CaCO_3$ content of up to 88% d. wt. Organic carbon was high, up to 3%, in the upper 15 cm, below which it dropped abruptly and remained around 0.6% down to 500 cm depth. Although the surface layer had relatively high organic content, it was not a typical sapropel and it had no varving.

3.2. Sulfur and Iron Geochemistry

The four stations, ranging from the oxic-anoxic shelf break to the sulfidic deep sea, showed similar patterns of zonation in sulfur geochemistry (Figs. 5–8). Sulfate reduction started at the sediment–water interface and was the dominant mineralization process down to the bottom of the sulfate zone (Weber et al., 2001; Jørgensen et al., 2001). Accordingly, sulfate decreased right from the sediment surface and penetrated a few meter or deeper subsurface to where methane accumulated. The methane gradients are shown only up to a few mM concentration, beyond which the methane escaped from the supersaturated sediment because of bubble and crack formation after core recovery. There was an unusually broad overlap between sulfate and methane at all stations. Yet, a diffusion-diagenesis modeling of the sulfate and methane profiles consistently showed an enhanced sulfate reduction in the zone of anaerobic methane oxidation (see data in Jørgensen et al., 2001).

The pore water H_2S reached a peak of 500–900 μM at the sulfate–methane interface, highest at the deeper stations where also the overlying seawater contained 100–300 μM H_2S. It was a striking observation that the H_2S concentration dropped steeply below the peak and reached zero at 250–380 cm depth where the H_2S met an opposed diffusion gradient of dissolved Fe^{2+} (analyzed only at Stations 5 and 7). Obviously, the H_2S is effectively drawn down to a reaction zone where it is completely trapped by iron.

FeS (AVS) was present at rather low and uniform concentrations, <5 μmol cm^{-3}, throughout most of the sediment. However, the deep H_2S-Fe^{2+} interface coincided with a sharp peak of FeS which was visible in all cores as a distinct black band in the otherwise gray Unit III sediment. Thus, the front of downwards diffusing H_2S caused a progressive sulfidization in the limnic deposit and precipitated as an X-ray amorphous iron sulfide. Above (i.e., behind) this progressing diffusion front, the FeS was converted into (or replaced by) pyrite, which is the more stable mineral phase.

The pyrite (CRS) concentration increased steeply with depth below the sediment surface and was high and mostly variable throughout most of the H_2S zone. At several stations pyrite reached a subsurface maximum in the sapropel layer at 30–50 cm depth. From ~0.5 m above the peak of the FeS band, pyrite dropped steeply with depth to reach a low background concentration of 2–5 μmol cm^{-3} in the nonsulfidized limnic sediment below the FeS band.

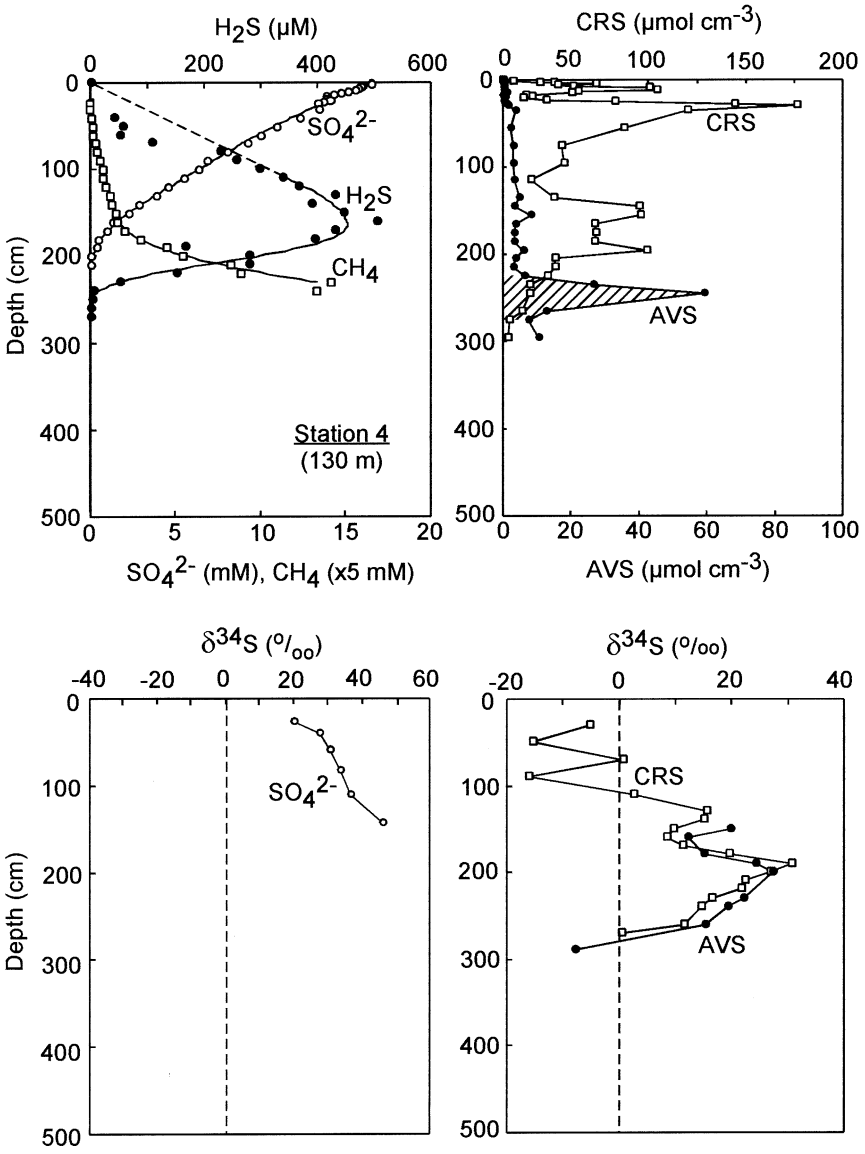

Fig. 5. Station 4, sulfur geochemistry: Upper left: SO_4^{2-}, H_2S, and CH_4 (notice scales) in the pore water. The smooth curves are model fits to the data based on the PROFILE model. Upper right: Acid volatile sulfide (AVS) and chromium reducible sulfur (CRS). Lower left: Sulfur isotopic composition of SO_4^{2-} in the pore water. Lower right: Sulfur isotopic composition of AVS (●) and CRS (□).

Between the black FeS band and the light-gray pyrite zone above, the sediments were visibly speckled with mm-size black dots. These were sulfide-enriched microenvironments of hydrotroilite or mackinawite precipitation embedding micronodules of greigite (Fe_3S_4). Greigite is a magnetic iron–sulfur mineral and, accordingly, the gray micronodules could be extracted from the sediment with a simple magnet. Their identity was confirmed by X-ray diffraction analysis and by scanning of the magnetic susceptibility in an intact gravity core from Station 7 (Neretin et al., submitted). Distinct peaks of magnetic susceptibility were observed in the sediment core at the depth of greigite occurrence (Neretin et al., submitted). The peaks reached a magnetic susceptibility of 9800 10^{-6} Sl at 340 cm depth over a background of ca. 100 10^{-6} Sl in the rest of the core. In the deeper limnic sediment, the FeS and FeS_2 concentrations were low and uniform and FeS was the predominant iron–sulfur mineral.

3.3. Sulfur Isotopes

The isotopic compositions of H_2S and SO_4^{2-} in the pore water are also shown in Figures 5–8 ($\delta^{34}S$ of H_2S available only for Stations 6 and 7). The $\delta^{34}S$ of both species increased steeply with depth with near-linear and parallel or converging gradients. In the sulfidic bottom water of the Black Sea, sulfate had an isotopic composition of +21‰ and H_2S of −38‰, i.e., a $\Delta^{34}S = 59‰$.

At Station 6 (Fig. 7), in the sapropel layer starting at 50 cm depth, the difference between the two species had increased to $\Delta^{34}S = 65‰$ (from –31‰ in H_2S to +34‰ in SO_4^{2-}). The

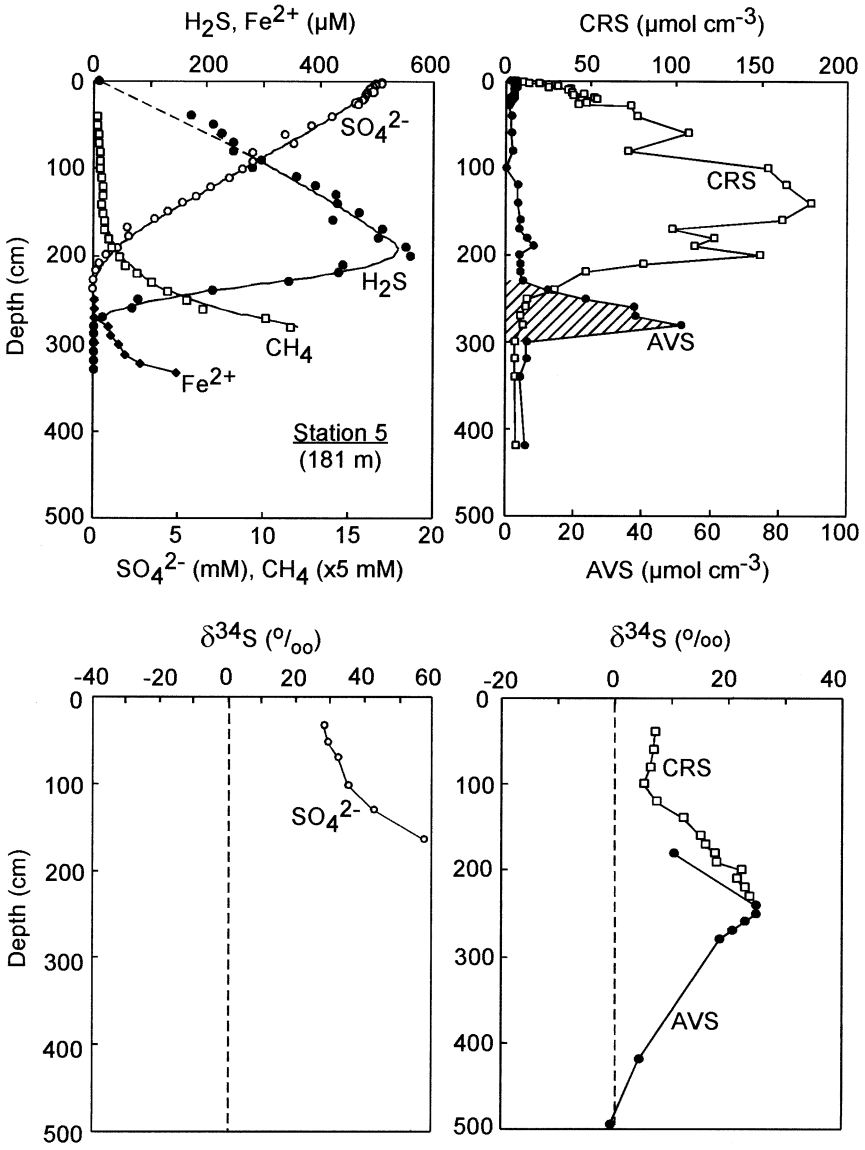

Fig. 6. Station 5, sulfur geochemistry (see legend of Fig. 5).

$\delta^{34}S$ of H_2S at Station 6 continued to increase down through the H_2S peak and reached +18‰ at 285 cm, at a depth where H_2S was no longer produced due to the absence of sulfate but diffused downward and precipitated in the black FeS band, which had a similar $\delta^{34}S$ of +16 to 18‰. The pyrite in the sapropel layer near the sediment surface was highly depleted in ^{34}S ($\delta^{34}S = -36.5$‰), which is typical for surface sediments of the Black Sea (Lyons, 1997). This pyrite was probably deposited from the water column or formed in the uppermost sediment layer by precipitation of ambient pore water H_2S which had a $\delta^{34}S$ of −30 to −40‰ (Neretin et al., 1998a). In the deposits below 140 cm depth, where the marine sulfidization front had penetrated down into formerly limnic sediment, the pyrite was extremely heavy, around +20‰.

At Station 7, the isotopic difference in the sapropel layer at 50 cm depth was even larger than at Station 6, from –26‰ in H_2S to +43‰ in SO_4^{2-}, i.e., $\Delta^{34}S = 69$‰ (Fig. 8). The SO_4^{2-}-H_2S difference even increased with depth to reach $\Delta^{34}S = 77$‰ (–4‰ to +73‰) at 310 cm. This is an extreme enrichment for sulfate, considering that 20% of the surface concentration was still remaining, and indicates that the isotopic fractionation was unusually high. Near the sediment surface, the pyrite had a $\delta^{34}S$ near −40‰, similar to the water column H_2S. Its isotopic composition fluctuated more with depth than at Station 6 and was around 0‰, similar to FeS, at the diagenetic front around 400 cm. A more highly resolved analysis of $\delta^{34}S$ in AVS, FeS_2, and S^o for a parallel core from Station 7 is presented in Neretin et al. (submitted).

At the shallow Station 4 the $\delta^{34}S$ of pore water sulfate similarly increased with depth to reach +47‰ at 150 cm, whereas at Station 5 it increased to +60‰ at 170 cm. The $\delta^{34}S$ gradients of pyrite and FeS were less extreme at Stations 4 and 5, yet the heaviest solid-phase sulfur was found at these stations, up to +24‰ for FeS and +30‰ for FeS_2 (Figs. 5 and 6).

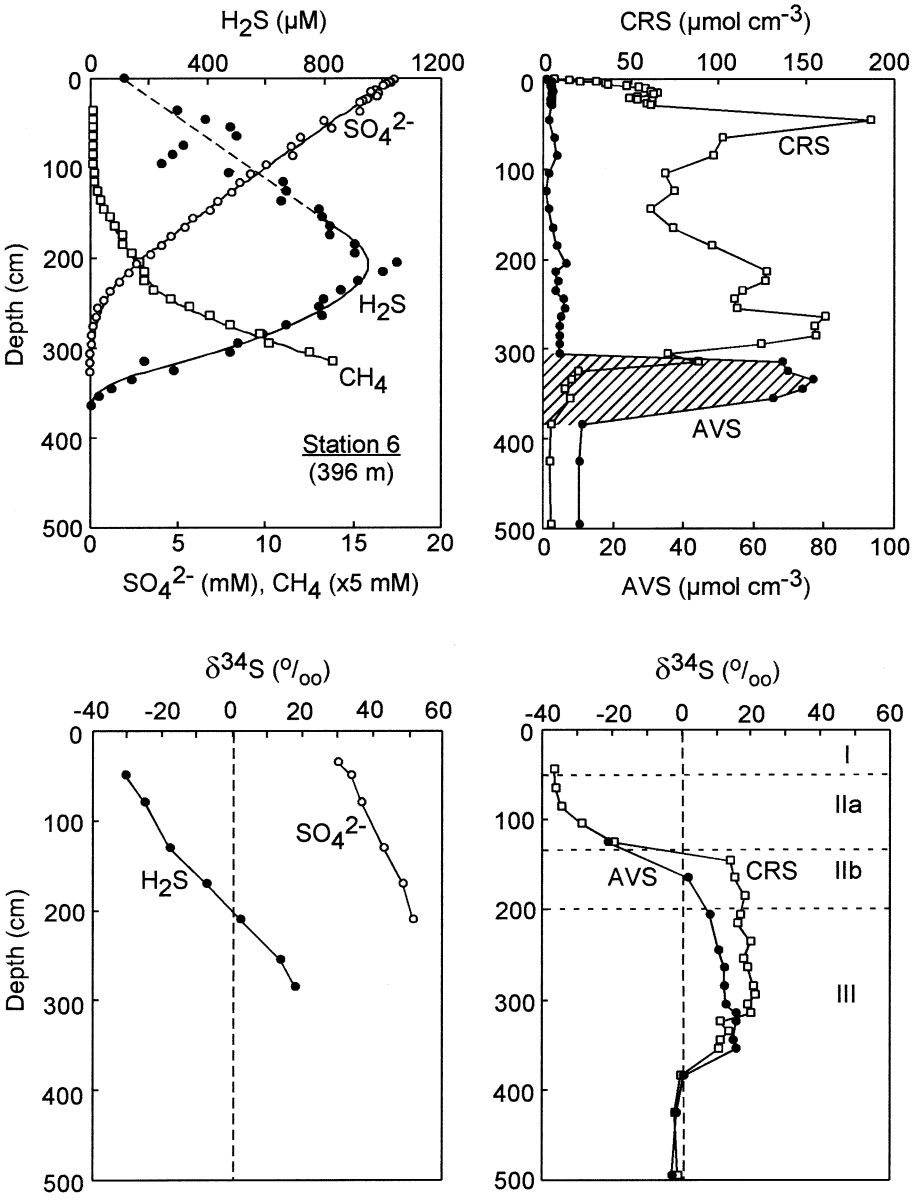

Fig. 7. Station 6, sulfur geochemistry (see legend of Fig. 5). The chronological units of the sediment are indicated in the lower right frame.

The fluctuating or positive $\delta^{34}S$ values for pyrite in the upper 100 cm at Stations 4 and 5 may be due to transport and redeposition of shelf sediment, thereby mixing formerly limnic and modern marine sediment, as also indicated by the presence of shells of freshwater bivalves here at the shelf break. It was characteristic for all stations that AVS and CRS had similar isotopic compositions just above the diagenetic front. Below this diagenetic front, where the limnic sediment was unaffected by a later marine overprinting, the $\delta^{34}S$ of both FeS and FeS_2 was lower at all stations with values around 0‰. This value is typical for lake sediments in which sulfate reduction is diffusion limited and there is consequently little net fractionation between lake water sulfate and sediment sulfides (Nriagu and Soon, 1985).

3.4. H_2S Dynamics

The net production and consumption rates of H_2S throughout the sulfide zone were calculated by modeling of the H_2S profiles. As examples, the results for Stations 5 and 6 are shown in Figure 9. The H_2S data are noisy, especially near the sediment surface where a linear interpolation was made to the accurately known H_2S concentration in the overlying water. Despite this noise, the depth-integrated rates calculated by the model are robust in the sense that they are governed by the flux upward to the sediment surface, the flux downward to the H_2S-Fe^{2+} interface, and the net production in between which balances these two fluxes. The model is internally consistent in that net production balances consumption and diffusion losses.

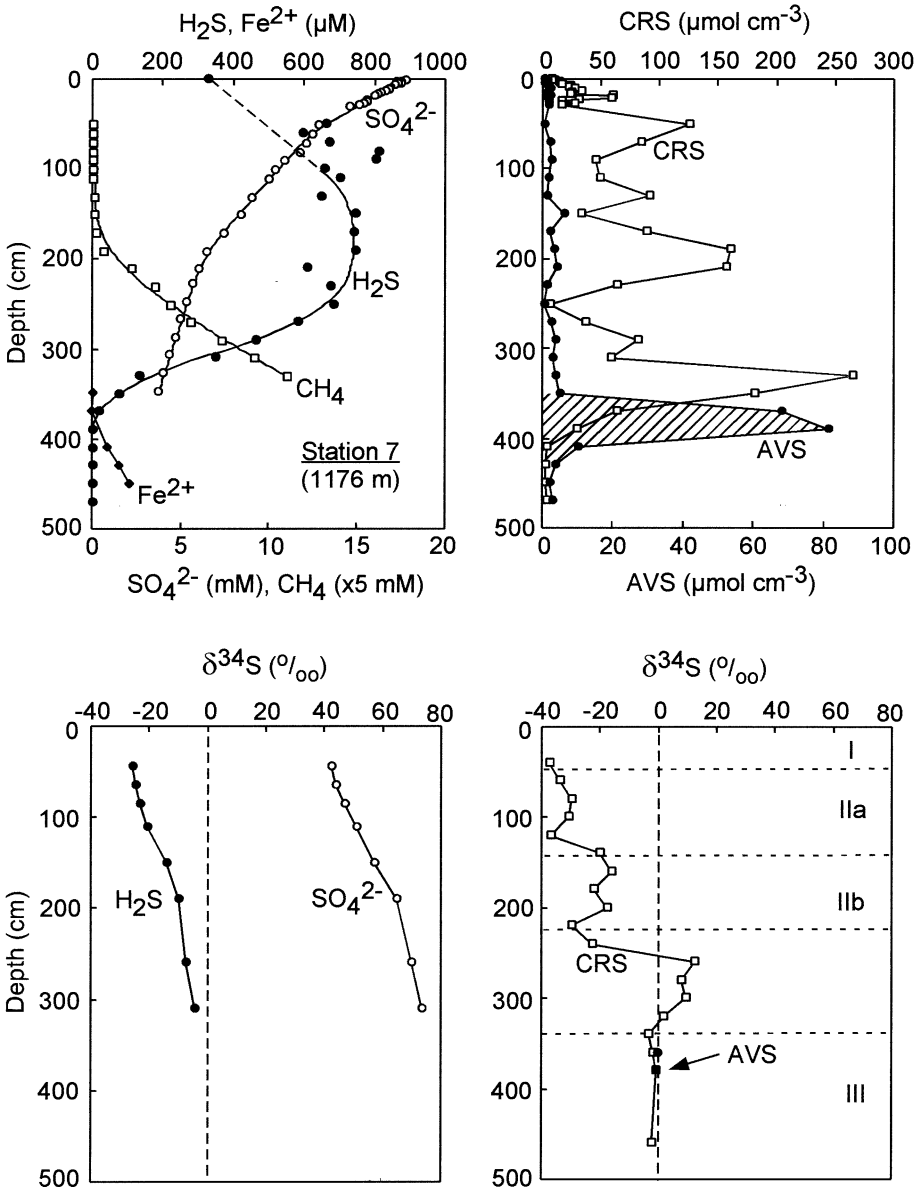

Fig. 8. Station 7, sulfur geochemistry (see legend of Fig. 5). The chronological units of the sediment are indicated in the lower right frame.

In Figure 9, the rates of net sulfate reduction are shown as calculated by similar modeling of the sulfate curves (data from Jørgensen et al., 2001). Highest sulfate reduction rates of around 0.15 nmol cm^{-3} d^{-1} were found at the depth of the sulfate–methane transition, where also the highest rates of net H_2S production occurred. The difference between the net sulfate reduction and the net H_2S production shows which fraction of the produced H_2S was trapped within the sulfide zone, mostly by pyrite formation. A smaller fraction may have been incorporated into the organic sulfur or elemental sulfur pools (see below).

The H_2S diffusing upward was lost to the overlying water column, and therefore only the flux was calculated from the model. The H_2S diffusing downward reacted with iron in a defined horizon, and this consumption rate could be modeled from the H_2S curve (negative rates in Fig. 9).

3.5. Iron and Sulfur Speciation

The depth distributions of solid-phase sulfur and iron species in the sediment showed similar trends at all stations and are shown only for Station 6 down to 850 cm depth in Figure 10. The left panel shows that the available iron had mostly reacted with sulfur above the sulfidization front down to 380 cm. In the marine to brackish deposits, which include the upper 200 cm (cf. Fig. 3), pyrite was the dominant sulfur–iron species. At 300–350 cm, the large pool of metastable FeS comprised 50%

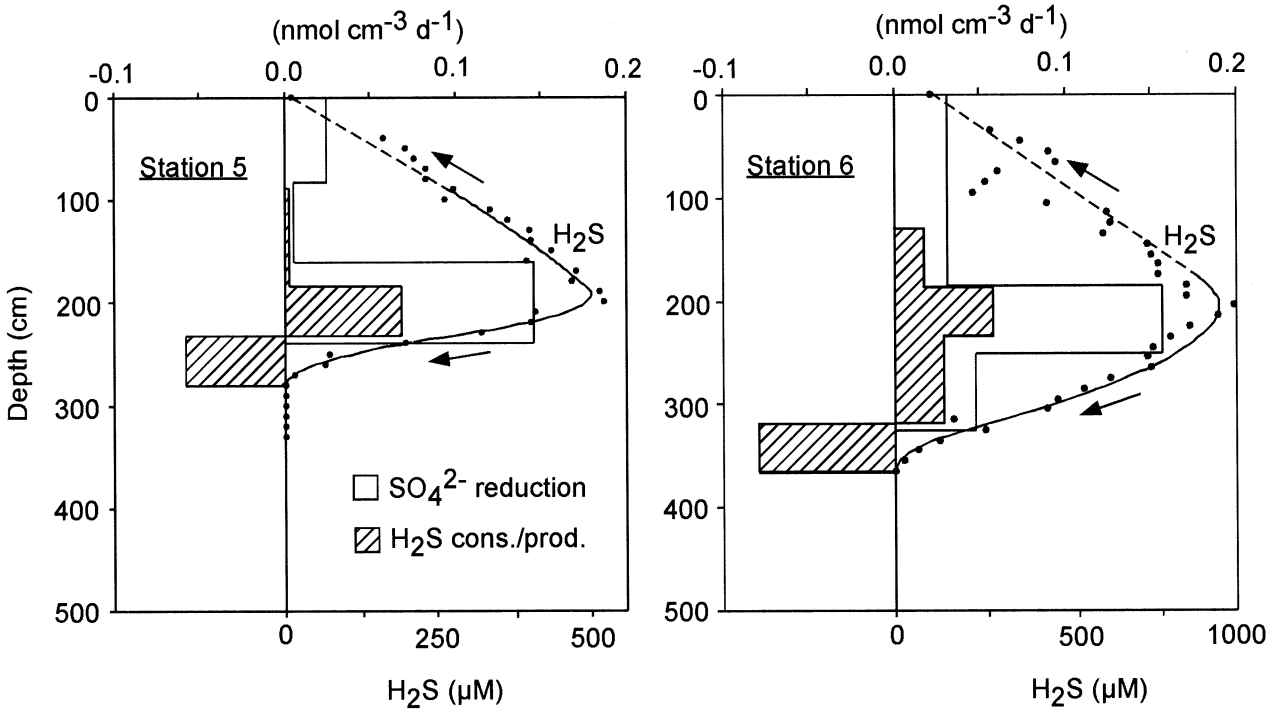

Fig. 9. Stations 5 and 6: Depth distributions of pore water H_2S concentrations and of modeled rates of net sulfate reduction (open bars) and of net H_2S production/consumption (cross-hatched bars; production = positive on the scale, consumption = negative on the scale). The H_2S reached a maximum at around 200 cm depth where the SO_4^{2-}-CH_4 interface was located. From there the H_2S diffused upward to the sediment surface, where it was lost to the water column, or downward to the H_2S-Fe^{2+} interface, where it was trapped as FeS.

of the total iron. In the limnic sediment below, most of the iron was present as non–sulfur-bound Fe(II+III).

Pyrite was the main sulfur pool above the diagenetic front (Fig. 10, right panel). In the sapropel, 70–90% of the sulfur was bound as pyrite whereas the rest occurred as organic sulfur. Also in the sulfidized limnic sediment, just above the black FeS band, pyrite dominated with smaller contributions from FeS and elemental sulfur. At the sulfidization front, 60% of all the sulfur was bound as amorphous FeS and only little had reacted further to pyrite. In the limnic sediment with low sulfur content, FeS and FeS_2 comprised around 40% each, whereas S° and organic sulfur accounted for around 10% each.

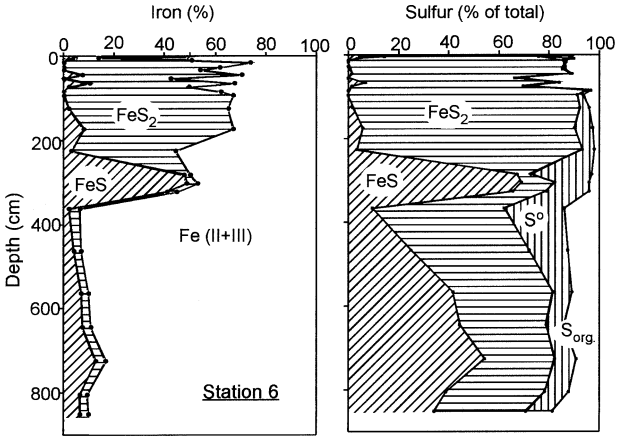

Fig. 10. Iron–sulfur geochemistry of sediment from Station 6. Left: Relative distributions of iron in three main pools of FeS, FeS_2, and reactive iron (i.e., non–sulfur-bound Fe(II) and Fe(III)). Right: Relative distributions of sulfur in the pools of FeS, FeS_2, S°, and S_{org}.

4. DISCUSSION

4.1. Dynamics of Sulfate and H_2S

In the following, the dynamic sulfur cycle in the Black Sea sediments is discussed with the aim to understand how open system diffusion and deep sources of methane and iron affect the distribution of sulfur species, their mass balance, and their isotopic signals.

4.1.1. Sulfate Penetration Depth

The depth distributions of SO_4^{2-} and H_2S result from the modern balance of sulfate reduction rates and sulfide sinks and from the diffusion fluxes of these pore water species. Their gradients vary on a much shorter time scale than the depositional history of the surrounding sediment. As the following calculations will show, the depth of sulfate penetration has been continuously regulated by the sulfate concentration in the Black Sea water throughout the Holocene and by the upward flux of methane. The H_2S distribution is, in addition to these two factors, regulated by its immobilization by iron and incorporation into solid-phase pools (FeS, FeS_2, S°, organic S). As an

Table 2. Dynamics of H_2S at its peak concentration

No.	Parameter	Station 4 (130 m)	Station 5 (181 m)	Station 6 (396 m)	Station 7 (1176 m)
1.	Depth of H_2S peak	160 cm	195 cm	210 cm	190 cm
2.	SRR (nmol cm^{-3} d^{-1})	0.158	0.145	0.157	0.057
3.	Porosity	0.58	0.55	0.70	0.68
4.	SRR (μM d^{-1})	0.298	0.274	0.224	0.084
5.	H_2S conc. (μM)	480	540	980	760
6.	Turnover time of H_2S	4 yr	5 yr	12 yr	25 yr

SRR = sulfate reduction rate.

example, the dynamics of SO_4^{2-} and H_2S are in the following calculated for Station 6. Results from all stations are summarized in Tables 2 and 3.

More than half of the entire sulfate reduction in the anoxic Black Sea sediments takes place in the uppermost 0–10 cm (Jørgensen et al., 2001). Yet, we suggest that it is the deep sulfate reduction, in particular at the sulfate–methane transition, which is the most important for the depth of sulfate penetration and for the quasi-linear shape of the sulfate profiles. In that case, the sulfate penetration depth, $Z_{sulfate}$, can be estimated from the rate of sulfate reduction in the sulfate–methane transition and from the sulfate concentration, C_0, at the sediment–water interface. The approximated flux, J, of sulfate to the sulfate–methane transition is:

$$J = \varphi D_s(C_0 - C_\infty)/Z_{sulfate} \quad (3)$$

where the flux is equivalent to the areal rate of sulfate reduction in the transition zone, and where the mean sulfate diffusion coefficient, D_s, as calculated from Eqn. 1, is 0.35 10^{-5} cm^2 s^{-1}. The sulfate concentration, C_∞, at the lower boundary is zero, so that:

$$J = \varphi D_s C_0/Z_{sulfate}, \quad \text{or} \quad (4)$$

$$Z_{sulfate} = \varphi D_s C_0/J. \quad (5)$$

For Station 6, C_0 was 17.2 mM (=17.2 μmol cm^{-3}), the modeled rate of sulfate reduction rate (SRR) in the whole sulfate–methane zone was 0.133 mmol m^{-2} d^{-1} (=1.54 10^{-7} μmol cm^{-2} s^{-1}), and the mean porosity was 0.7. Accordingly, the sulfate penetration depth should be: $Z_{sulfate}$ = (0.7 0.35 10^{-5} 17.2)/(1.54 10^{-7}) = 280 cm. The actual penetration depth is 250–300 cm (Fig. 7). This simple comparison shows that the deep methane-driven sulfate reduction is the most important in governing the depth of sulfate penetration today.

4.1.2. Sulfate Dynamics

In accordance with Eqn. 5, the depth of the sulfate zone varies roughly in proportion to the sulfate concentration at the sediment surface and, with approximation, in inverse proportion to the upward methane flux. The sulfate concentration has expectedly changed during the Holocene with changing salinity in the deep Black Sea. The methane flux, we presume, has been rather constant or decreased slowly over time, as the methane originates from carbon degradation in old Pleistocene deposits unaffected by Holocene changes. Sodium chloride and other sea water ions started to penetrate into these deposits after the opening of the Bosporus (Jørgensen et al., 2001), and this must have forced the microbial populations to change from freshwater to marine strains. Yet, methanogenesis must have remained the terminal mineralization process below the sulfate zone and its rate remained a function of organic matter reactivity. Only in the uppermost meters of the Pleistocene sediment did mineralization shift to sulfate reduction.

The characteristic time, t, required for adjustment of the sulfate gradient when either of these key parameters changed in the past depends on the diffusion time of sulfate from the sediment surface to the depth of sulfate penetration, $Z_{sulfate}$. This time can be calculated from the Einstein-Smoluchowski relation: $t = L^2/2D_s$ (where L is the standard deviation by diffusion in a normal distribution of diffusion distances). The time can also be calculated from the modified relation (Sten-Knudsen, 1995): $t = \pi L^2/4D_s$ (where L is the *mean* deviation by diffusion). The depth of the sulfate zone at Station 6 was ca. 280 cm and the mean diffusion time is, accordingly, $t = (\pi 280^2)/(4 \cdot 0.35\ 10^{-5}) = 2.0\ 10^{10}$ s = 560 yr. A change in sulfate concentration of the bottom water in the Black Sea will consequently lead to an adjustment of the entire sulfate zone within ~500 yr, which is a short period relative to the salinity development of the Black Sea during the Holocene. The main salinity increase in the water column may have taken place over the first 2000–3000 yr after the opening of the Bosporus and may subsequently have been rather constant over the last ca. 7000 yr. Thus, it is likely that the depth of the sulfate–methane interface has also been rather stable, balanced in quasi-steady-state between the fluxes of methane and sulfate.

4.1.3. H_2S Dynamics

The H_2S in the pore water varies on a much shorter time scale than sulfate because it is in a dynamic equilibrium between its production from sulfate reduction and its removal by immobilization and diffusion loss. The peak of H_2S concentration at Station 6 was reached within the sulfate–methane transition at a depth of 210 cm (Fig. 7, Table 2 *(1)*; numbers in *italics* refer to the line number in Table 2). The rate of sulfate reduction (and thus the gross rate of H_2S production) at the sulfate–methane transition can be calculated from diffusion-diagenesis modeling of the pore water sulfate gradient. The highest rate of sulfate reduction (SRR) occurred at 200–260 cm and was 0.157 nmol cm^{-3} d^{-1} (Fig. 9, Table 2 *(2)*). By a porosity of 0.70 *(3)*, this corresponds to a rate of (0.157/0.70=) 0.224 μM SO_4^{2-} d^{-1} *(4)* when calculated on a pore water basis. As the peak H_2S concentration was 980 μM *(5)*, the turn-over time of H_2S is (980/0.224=) 4400 d or 12 yr *(6)*. Thus, the entire pool of H_2S deep in the sediment is renewed within 12 yr. Accordingly, the entire pore water profile of H_2S will adjust within less than a decade to any changes in its production or removal.

Similar calculations made for the other stations provide similar results (Table 2). At the shallower stations, the depth of sulfate penetration was shallower (Figs. 5 and 6), the sulfate gradients were steeper, and the diffusion dynamics were correspondingly faster. At the deep Station 7, the bottom of the sulfate zone was not reached by the gravity corer.

In conclusion, the turn-over time of H_2S at peak concentration in the pore water *(6)* increased with water depth from 4 yr

Table 3. Budgets for methane-driven H_2S production and fluxes. Process rates or fluxes are all in units of mmol m^{-2} d^{-1} (if not in %, as indicated).

No.	Parameter	Station 4 (130 m)	Station 5 (181 m)	Station 6 (396 m)	Station 7 (1176 m)
1.	SRR in CH_4 oxidation zone[a]	0.111	0.116	0.133	0.110
2.	Net H_2S prod. in CH_4 zone	0.029	0.035	0.049	0.047
3.	Net H_2S prod., % of SRR	26%	30%	36%	42%
4.	H_2S flux up to surface	0.008	0.008	0.017	0.023
5.	H_2S flux down to Fe^{2+}	0.021	0.027	0.032	0.024
6.	Loss of H_2S in CH_4 oxid. zone	0.082	0.081	0.084	0.063
7.	Total SRR in whole sulfate zone[a]	0.65	1.43	0.74	0.73
8.	H_2S flux down, % of Total SRR	3.2%	1.9%	4.3%	3.3%
9.	CH_4 oxidation[a]	0.113	0.097	0.083	0.048
10.	H_2S flux down, % of CH_4 oxid.	19%	28%	39%	50%
11.	H_2S flux down, % of SO_4^{2-} flux	7%	24%	15%	10%

[a] Data from Jørgensen et al. (2001).

at Station 4 to 25 yr at Station 7. Thus, the H_2S pool is extremely dynamic, much more than the vast pool of H_2S in the water column which has an estimated turn-over time of 90–150 yr (Skopintsev, 1975; Neretin et al., 2001) or even longer, 890 yr according to Albert et al. (1995).

4.2. Budgets for Methane-driven H_2S Production

Similar to the driving force for the sulfate gradient, the flux of H_2S up toward the sediment surface is to a large extent governed by methane-driven sulfate reduction deep within the sediment. To compare the process rates and fluxes of the combined SO_4^{2-}-H_2S-CH_4 system, mass balance calculations are made in the following, with Station 6 again serving as the example. Results for all four stations are compiled in Table 3.

At Station 6, the zone with enhanced sulfate reduction rates, primarily fueled by methane, extended over the depth interval of 195–325 cm, i.e., over a 130-cm-thick sediment zone (Figs. 7 and 9). (The entire sulfate–methane interface started already at 120 cm depth, yet the upper 75 cm of the methane zone had only a moderate effect on the sulfate gradient). The depth-integrated net sulfate reduction within this 130-cm interval, 0.133 mmol m^{-2} d^{-1} (Table 3, *(1)*), was calculated for the two rate intervals between 195 and 325 cm from the product of rates in nmol cm^{-3} d^{-1} and depth interval in cm, thus providing areal rates in nmol cm^{-2} d^{-1} which can be converted to mmol m^{-2} d^{-1} by dividing by 100. Out of those 0.133 mmol m^{-2} d^{-1} of H_2S formed, A) some diffused up toward the sediment surface, B) some diffused down toward the hydrotroilite band at the H_2S-Fe^{2+} interface, and C) some was trapped within the interval by precipitation with iron, or by immobilization as elemental or organic sulfur. The net H_2S production as modeled from the H_2S profile was 0.049 mmol m^{-2} d^{-1} *(2)* or 36% *(3)* of the net sulfate reduction in the sulfate–methane transition. The upward diffusion was 0.017 mmol m^{-2} d^{-1} *(4)* or 13% of the net sulfate reduction. The downward diffusion was 0.032 mmol H_2S m^{-2} d^{-1} *(5)* or 24%, which leaves (0.133–0.017–0.032=) 0.084 mmol H_2S m^{-2} d^{-1} *(6)* or 64% for reaction and precipitation within the depth interval. The (0.017+0.032=) 0.049 mmol m^{-2} d^{-1} of H_2S, which diffused away from the H_2S peak, corresponds to the modeled net production of H_2S within the sulfate–methane transition (Table 3 *(2)*). Thus, the H_2S model is internally consistent. The calculated relative allocations of H_2S are also robust because they are based on simple pore water profiles using the same diffusional transport modeling for both SO_4^{2-} and H_2S.

The results are surprising in several ways. They show that the H_2S diffusing up to the sediment surface and into the water column from deeper sediment layers is a very small fraction, 13%, of the H_2S production down there. Twice as much of the deep H_2S production, 24%, is drawn downward to be immobilized by iron at the diagenetic front. Nearly two-thirds, 64%, of all the H_2S produced at the sulfate–methane interface is trapped within that zone. A similarly high fraction of internal sulfide trapping and reoxidation, 34% to 80%, was calculated for sapropels of the eastern Mediterranean (Passier et al., 1999).

It is important to note that a modeling of the H_2S profile shows the dynamics of only those 36% of the produced H_2S which did not become immobilized within the boundaries of the H_2S zone (therefore the term "net H_2S production"). The immobilization was mainly due to reaction with iron and partial or complete reoxidation of the sulfide. Accordingly, the originally deposited reactive Fe(III) within the limnic sediment down to 350 cm had been mostly reduced by H_2S and bound in FeS or FeS_2. Below that depth, however, the reactive iron concentration was still high, 1.1–1.5% d.w. (Neretin et al., submitted), and much of it occurred as Fe(III). This shows that the reactive iron pool had remained unreacted in the limnic deposit for several tens of thousands of years until it was attacked and reduced by the downwards progressing H_2S front.

All these calculations comprise only sulfate reduction within the sulfate–methane transition. The total sulfate reduction rate (total SRR) from the sediment surface to the bottom of the sulfate zone was found by adding experimentally measured rates in the upper 15 cm and modeled rates below 15 cm. At Station 6 the total SRR was 0.74 mmol m^{-2} d^{-1} (Table 3 *(7)*). Thus, the downward flux of H_2S, which leads to the distinct iron sulfide band below 300 cm, comprises a H_2S loss of only 4.3% *(8)* of the entire H_2S production. Yet, this relatively small loss has profound consequences for the sulfur mass balance of the sediment and for its sulfur isotope geochemistry. The H_2S is almost entirely derived from methane-driven sulfate reduction which was 0.083 mmol m^{-2} d^{-1} *(9)*, as calculated from the modeled rate of methane oxidation (Jørgensen et al., 2001). When calculated relative to the methane-driven H_2S production alone, however, the downward flux comprised a large fraction, 39% *(10)*. When compared to the sulfate flux across the sediment–water interface (data from Table 3 *(4)* in Jørgensen et al., 2001), the deep H_2S sink comprised 15% (Table 3 *(11)*).

A comparison of such data for the four Black Sea stations shows clear trends from the shelf edge to the deep sea (Table 3). With increasing water depth, the net H_2S production comprised an increasing fraction of the net sulfate reduction in the methane–sulfate transition zone, from 26% to 42% (Table 3 *(3)*). The H_2S flux up toward the sediment surface increased

with depth *(4)*, whereas the flux down toward the black FeS band was more constant *(5)* and comprised between 1.9% and 4.3% of the total sulfate reduction in the sediment *(8)*. Compared to the methane-driven sulfate reduction *(9)*, however, the downward H_2S flux increased in importance from 19% at the shelf break to 50% in the deep basin *(10)*.

4.3. Dynamics of FeS and FeS_2

The black band of hydrotroilite at several meters sediment depth was a distinct geochemical feature at all four stations investigated. As shown in the following, this narrow zone of FeS precipitation at the interface between counter-diffusing H_2S and Fe^{2+} must have formed during a period in the late Holocene where the diffusion front was moving only very slowly. To understand the dynamics and rate of hydrotroilite and pyrite formation, data from Station 6 are again used as an example.

4.3.1. Pyrite Formation

The rate of pyrite formation within the sulfate–methane transition will first be calculated. The sediment below 200 cm depth, which represents deposits from the freshwater period, has been penetrated by sulfate and other seawater ions during the Holocene. The diffusion front, which has left behind (above) it a typical marine sulfur geochemistry, is presumably still today progressing into the limnic sediment and slowly pushing down the two opposing diffusion fronts of SO_4^{2-}-CH_4 and H_2S-Fe^{2+}. The iron-sulfide minerals are currently being added to a small background of pyrite which formed during the sulfur-limited limnic stage, >9800 yr ago. To calculate only the FeS_2 formed during the later marine period, the small limnic background of ca. 5 μmol FeS_2-S cm^{-3} is, therefore, first subtracted. The marine pyrite pool, which has formed within the present-day sulfate–methane interface, increases with depth down through the diagenetically altered, limnic Unit III (Figs. 3 and 7) and averages 92 μmol S cm^{-3}. For the 130-cm-thick zone, this amounts to $130 \times 92 = 11{,}900$ μmol S cm^{-2} = 119,000 mmol S m^{-2}. Given a total H_2S immobilization rate within this zone of 0.084 mmol m^{-2} d^{-1} (Table 3 *(6)*), the minimum time, T_{min}, required to build up the pyrite pool at the present-day rate can be calculated:

$$T_{min} = 119{,}000 \text{ mmol } m^{-2}/0.084 \text{ mmol } H_2S \text{ } m^{-2} \text{ } d^{-1} = 1.42 \text{ } 10^6 \text{ days} = 3900 \text{ years} \quad (6)$$

Thus, if all the H_2S immobilized within the sulfate–methane interface had been used to form pyrite, the present pyrite pool should at steady state have taken ~3900 yr to form. Because pyrite was by far the dominant form of solid-phase sulfur forming postdepositionally within that depth interval, this estimate should be realistic.

4.3.2. FeS Formation

A similar calculation can be made for the sharply bounded, black FeS layer which at Station 6 occurred below the pyrite zone at 310–360 cm depth (Fig. 7). Within this 50-cm-thick zone, the mean FeS concentration was 71 μmol S cm^{-3}. Pyrite is here less important and not much above the limnic background throughout most of the interval. The total FeS pool is thus $50 \times 71 = 3540$ μmol cm^{-2} or 35,400 mmol m^{-2}. Because the FeS zone is situated below the sulfate zone, there is no dissimilatory H_2S production within the layer and the supply of H_2S for its formation comes exclusively from H_2S diffusing downward from the H_2S peak. The maximum below-peak gradient of H_2S is 7.1 μM cm^{-1} and the sediment diffusion coefficient of H_2S is, $D_s = 0.65 \text{ } 10^{-5}$ cm^2 s^{-1}. The downward diffusion flux of H_2S into the FeS zone is thus:

$$J(H_2S_{down}) = \varphi D_s dC/dz = 0.70 \times 0.65 \text{ } 10^{-5} \times 7.1 \text{ nmol } cm^{-2} \text{ } s^{-1} \quad (7)$$

If this H_2S flux supplied all sulfide for the FeS band, then the time, T, required to transfer the corresponding amount of sulfide can be calculated from the FeS pool size divided by the H_2S flux:

$$T = 35{,}400 \text{ mmol } m^{-2}/0.032 \text{ mmol } m^{-2} \text{ } d^{-1} = 1.11 \text{ } 10^6 \text{ days} = 3030 \text{ years} \quad (8)$$

The time required to form the FeS band is thus of similar magnitude as the formation time of the pyrite pool. For the shallower Stations 4 and 5, similar calculations yielded shorter formation times of the FeS pool of around 1500 yr, whereas at Station 7 it was 2700 yr (data not shown).

Marine sedimentation has continued in the euxinic Black Sea basin during these several thousand years of FeS and FeS_2 formation. The mean sedimentation rate over the entire marine period of 9800 yr was 16 cm/1000 yr. Within the last 3000 yr, the sediment surface has thus moved up by ca. 50 cm (cf. Fig. 3), which is little relative to the present depth of the sulfate zone of 280 cm. Consequently, even small changes in salinity and sulfate concentration of the Black Sea water may have played a larger role for the depth of sulfate penetration, and thus for the depth of the black FeS band, than the accretion of 50 cm sediment (cf. Eqn. 4).

The top 50 cm of sediment corresponds to the thickness of Unit I (Fig. 3). The Unit I/II transition marks the (re-)introduction of coccolithophorids in the Black Sea and, thus, about 3000 yr of sedimentation according to the stratigraphic chronology (Hay et al., 1991). It is not possible to conclude whether the position of the narrow (<20 cm thick) H_2S-Fe^{2+} interface has moved up or down during the ca. 3000 yr while it formed a 50-cm-thick FeS band. However, since the dominant coccolithophorid, *Emiliania huxleyi*, does not grow at salinities below 11 (Bukry, 1974), the salinity should have exceeded this threshold which is 60% of the present surface water salinity. It may thus be assumed that also the sulfate concentration in the Black Sea was >60% of the present level over the last 3000 yr. If the sulfate concentration in the Black Sea has thus been relatively constant for several thousand years, also the depth of the sulfate zone has expectedly been relatively constant, because it is governed primarily by the methane flux and not by sulfate reduction near the sediment surface. The methane comes from deeper sources in the limnic sediment, at >300 cm, and its flux from below is not likely to be affected by short-term changes above that depth. In conclusion, it is quite plausible that the H_2S-Fe^{2+} interface has persisted around its present

depth long enough to build up the observed FeS band at the calculated rate.

4.3.3. H_2S-Fe^{2+} Counter-diffusion

If the black FeS band had formed exclusively by counter-diffusing H_2S and Fe^{2+}, the Fe^{2+} gradient required to stoichiometrically balance the H_2S flux at steady state can be calculated. We assume the simple precipitation:

$$H_2S + Fe^{2+} \rightarrow FeS + 2H^+ \quad (9)$$

Equal fluxes downward of H_2S and upward of Fe^{2+} require that:

$$J(H_2S) = J(Fe^{2+}) \text{ or}$$

$$D_s(H_2S)/dz = D_s(Fe^{2+})d[Fe^{2+}]/dz \quad (10)$$

By rearranging, the pore water gradient of Fe^{2+} should be:

$$d[Fe^{2+}]/dz = d[H_2S]/dz*D_s(H_2S)/D_s(Fe^{2+}) \quad (11)$$

where $d[H_2S]/dz$ is 9.8 μM cm^{-1} and $D(H_2S)$ and $D(Fe^{2+})$ are 1.22 10^{-5} cm^2 s^{-1} and 0.43 10^{-5} cm^2 s^{-1}, respectively, at 9°C (Schulz, 2000). Their ratio is presumably independent of the porosity. The required maximum Fe^{2+} gradient is then 28 μM cm^{-1}.

The Fe^{2+} gradient was measured only at Stations 5 and 7 where it was much lower than the equivalent H_2S gradient, 1–2 μM cm^{-1} for Fe^{2+} vs. 7–10 μM cm^{-1} for H_2S. Fe^{2+} diffusion thus appears to supply only a fraction of the iron required for FeS precipitation (Figs. 6 and 8). However, the data comprise only the very top of the Fe^{2+} zone and the extension of the gradient at depth is therefore poorly constrained.

The depth distribution of solid-phase iron in the limnic sediment provided independent evidence that only part of the iron for FeS formation in the black band was supplied by diffusion of Fe^{2+} from below. Both the total iron and the reactive iron remained rather constant with depth below 200 cm, and there was no distinct iron peak at around 300 cm depth, which could indicate that the Fe^{2+} flux caused a major accumulation of iron in the black band (Lüschen, 1998; data not shown). Based on the solid-phase pools alone, all the FeS could, in principle, have been derived from the available iron pool within the same depth interval. The progressing H_2S front is thus partly governed by slow dissolution-reduction of iron at the front and partly by dissolved iron diffusing up from the deeper limnic sediment. The Fe^{2+} diffusion flux retards the progression of the diagenetic front but does not entirely control it.

Calculations of the AVS and pyrite dynamics for the other three stations provided rather similar results.

Below the H_2S zone at Station 7 we also observed a pore water gradient of Mn^{2+} which, however, was only 15% of the Fe^{2+} gradient and therefore had only a minor potential role for sulfide immobilization. (M. E. Böttcher, unpublished data).

The FeS accumulation within a single black band was consistent in all the cores studied here. In other parts of the Black Sea, however, the band is split up into several or many layers (Berner, 1974; Arthur and Dean, 1998). These were described as Liesegang bands by Berner (1969), who made experiments and subsequently made model calculations based on different scenarios of high vs. low sulfide and iron. The zonation observed here corresponds to his "intermediate" situation of counter-diffusing H_2S and Fe^{2+} by which distinct FeS bands are formed.

4.4. Sulfur Mass Balance

A mass balance of the modern sulfur cycle in Black Sea sediments will be calculated for Station 6 as an example. The rate of sulfur accumulation in the sediment can be estimated from the three main mechanisms of immobilization: 1) The deposition of sulfur and the recent accumulation of authigenic pyrite in the surface sediment; 2) the sulfidization of former limnic sediment in the zone of high H_2S above the FeS band; 3) the downward flux of H_2S and formation of an FeS band where the opposed diffusion gradients of H_2S and Fe^{2+} meet.

1) Pyrite in the upper 30 cm of modern coccolith ooze at Station 6 builds up steeply below the sediment surface to a mean concentration of 60 μmol FeS_2-S cm^{-3} (Fig. 7). This corresponds to 85% of the total sulfur in that layer, which is thus 70 μmol S cm^{-3}, the remaining sulfur being organically bound (Fig. 10). The mean sedimentation rate at Station 6 during the marine stage of Unit I+II was 0.17 mm yr^{-1}, and the rate of sulfur accumulation is thus 70 $\times$ 0.017 = 1.19 μmol cm^{-2} yr^{-1} or 0.033 mmol S m^{-2} d^{-1}.
2.) The current rate of sulfidization within the limnic sediment layer of 150–320 cm depth is 0.084 mmol S m^{-2} d^{-1} (Table 3 *(6)*).
3.) The downward diffusion of H_2S and its immobilization as FeS is 0.032 mmol S m^{-2} d^{-1} (Table 3 *(5)*).

The total accumulation of sulfur in the sediment is thus 0.033 + 0.084 + 0.032 = 0.149 mmol S m^{-2} d^{-1}, of which only 22% is due to modern surface deposition of pyrite and organic sulfur as well as authigenic pyrite formation in the coccolith ooze. The remaining 78% of sulfur accumulation currently takes place by deep sulfide immobilization within the old limnic sediment. As the total sulfate reduction rate integrated through the whole sulfate zone is 0.74 mmol m^{-2} d^{-1}, the current sulfur accumulation corresponds to 20% of the sulfur cycling on an areal basis.

The 0.033 mmol S m^{-2} d^{-1} of total sulfur accumulation in the upper Unit I+II layers slightly exceeds the sedimenting flux of total inorganic sulfur, 0.025 mmol S m^{-2} d^{-1}, found in sediment traps by Muramoto et al. (1991), mostly in the form of pyrite and elemental sulfur. In a study of the size distribution and morphology of pyrite in the eastern Black Sea basin, Wilkin and Arthur (2001) observed a dominance of framboidal pyrite in Unit I and II deposits and concluded that it originated mostly from syngenetic pyrite formed in the water column. A similar conclusion was reached by Canfield et al. (1996) who expected that the reaction kinetics of H_2S with Fe-containing silicates in the surface sediment would be too slow to explain the early pyrite accumulation. Elemental sulfur was insignificant in the Holocene marine deposit studied here (Fig. 10).

Similar calculations for the other stations yield similar general conclusions (cf. Figs. 5, 6, 8 and Table 3). At Station 7 in the deep basin, the mean total sulfur concentration was 80 μmol S cm^{-3} in the marine deposit which accumulated at a mean rate of 0.19 mm yr^{-1}. The rate of sulfur accumulation

from sedimentation and pyritization of the modern marine deposit was thus 0.042 mmol S m^{-2} d^{-1}. The sulfidization within the limnic sediment, where sulfate reduction currently takes place, was 0.063 mmol S m^{-2} d^{-1} while the downward H_2S diffusion to the black FeS band was 0.024 mmol S m^{-2} d^{-1}. The total sulfur accumulation was thus 0.129 mmol S m^{-2} d^{-1} of which 33% took place in the marine surface deposit and 67% in the deep limnic deposit. For comparison, Lein and Ivanov (1991) estimated sulfur accumulation rates in sediments of the western Black Sea to be 0.023–0.18 mmol S m^{-2} d^{-1}. Our data fall in the middle of that range.

The total sulfur accumulation at Station 7 corresponds to 18% of the total sulfate reduction, i.e., the same fraction as at the shelf station. This fraction is similar to other ocean margin sediments where generally 5–20% of the produced H_2S is bound as pyrite (Jørgensen et al., 1990), although a much higher fraction may be bound in rapidly accumulating sediments with high reactive iron content (Chanton et al., 1987a). These calculations show that the excess of reactive iron present today in the limnic deposits below 150 cm depth acts as an efficient sulfide trap. This deep sulfide sink draws down and immobilizes 7–24% of the sulfur which diffuses in as sulfate across the sediment–water interface (Table 3 *(11)*).

4.5. Sulfur Isotopes

The isotopic compositions of SO_4^{2-}, H_2S, FeS, and FeS_2 in the deep sediment cores showed similar patterns for the four stations ranging from the shelf break to the deep sea. The data raise several interesting questions concerning the mechanisms of isotope fractionation and the role of diffusion vs. immobilization for the resulting isotope signal of sediment sulfur:

- What is the isotopic mass balance of SO_4^{2-} and H_2S diffusion across the sediment–water interface? In other words, how can a downward flux of sea water sulfate, which has a $\delta^{34}S$ of +20‰, be converted into pyrite with a $\delta^{34}S$ of around −35‰ in the upper meter of sediment?
- What is the isotopic composition of the vertical fluxes of SO_4^{2-} and H_2S around the sulfate–methane interface where pyrite is formed with a $\delta^{34}S$ of +20‰?
- Why is the pyrite, which forms at depth in the Black Sea sediments, so extremely enriched in ^{34}S relative to other marine sediments? Is this an indication of closed system diagenesis, or does it relate to the deep Pleistocene sediments and the transition from limnic to marine conditions?

Again, data from Station 6, which are representative of all the stations, will be used as an example to answer these questions.

In the upper Holocene sediment, the pyrite had a sulfur isotopic composition of around −35‰, which is close to the $\delta^{34}S$ of –38 to −40‰ of H_2S in the deep water column (Neretin et al., 1998a) and –37.6‰ (range 32.7–39.4‰) measured in sedimenting pyrite (Muramoto et al., 1991). The pyrite sedimentation measured by those authors, ca. 0.025 mmol m^{-2} d^{-1}, corresponded to most of the sulfur accumulation in the marine deposit (cf. calculations in Section 4.4).

The modeling of the H_2S profile showed that an enhanced, methane-driven H_2S production occurred at the H_2S peak between 129 and 325 cm depth in the sediment of Station 6 (Figs. 7 and 9). An isotopic mass balance of sulfur was therefore made for the entire sediment column below 129 cm depth (Fig. 11) using the diffusion-diagenesis isotope model of Jørgensen (1979).

First, the isotopic difference between H_2S and SO_4^{2-} was very large throughout the sediment (Fig. 7). Jørgensen (1979) showed that a high degree of sulfide retention through pyrite formation leads to an isotopic difference between coexisting SO_4^{2-} and H_2S which is similar to the isotope fractionation by sulfate reduction. As the difference in the four Black Sea sediments remained mostly around $\Delta^{34}S \cong 60‰$, either the isotope fractionation during sulfate reduction was of this magnitude or additional fractionation mechanisms were involved. One such mechanism could be the partial reoxidation of sulfide to elemental sulfur by Fe(III) and the subsequent disproportionation of S°. Such a mechanism was suggested by Passier et al. (1999) to explain the accumulation and isotopic composition of pyrite in sapropels of the eastern Mediterranean. As shown by Canfield and Thamdrup (1994) and Böttcher et al. (2001), elemental sulfur disproportionation is associated with significant isotopic fractionation, producing relatively heavy sulfate and light sulfide. As the above calculations show, there was extensive reaction between sulfide and iron in the limnic sediment which could support such a S° formation and disproportionation-induced fractionation. The decreasing isotopic difference between SO_4^{2-} and H_2S with depth at Station 6 may thus be due to a decreasing primary fractionation by sulfate reducers or a decreasing role of disproportionation with depth.

According to model calculations, the sulfate flux downward across the 129 cm depth interface was 0.133 mmol SO_4^{2-} m^{-2} d^{-1} (Table 3 *(1)*; Fig. 11). This flux was equal to the net sulfate reduction in the sediment interval from 129 cm depth to the bottom of the sulfate zone at 325 cm depth. Most of the H_2S produced from this sulfate reduction was trapped by iron, either within the same sediment interval or upon diffusion downward to the H_2S-Fe^{2+} interface. Only 0.017 mmol H_2S m^{-2} d^{-1} diffused back up towards the sediment surface across the 129-cm interface. The isotopic composition at 129 cm depth was +43‰ for the pore water SO_4^{2-} and −15‰ for the H_2S (Figs. 7 and 11). The $\delta^{34}S$ of both species increased with depth with a $\delta^{34}S$ gradient of +0.123‰ cm^{-1} for SO_4^{2-} and +0.215‰ cm^{-1} for H_2S, as calculated by linear regression from the data in Figure 7. The values at the bottom of the sulfate zone at 285 cm depth were +60‰ for SO_4^{2-} (extrapolated from the linear regression; the sulfate concentration was too low for isotopic analysis at that depth) and +18‰ for H_2S (measured data).

4.5.1. $\delta^{34}S$ of Diffusing Sulfate

From the model fit to the SO_4^{2-} profile (Fig. 7), the concentration gradient at 129 cm depth was calculated. Using the combined concentration and isotope data, the separate diffusion fluxes of $^{32}SO_4^{2-}$ and $^{34}SO_4^{2-}$ could subsequently be calculated (cf. Jørgensen, 1979). The diffusion coefficients of the two species, $^{32}SO_4^{2-}$ and $^{34}SO_4^{2-}$, were assumed to be identical. From the ratio of the fluxes of the two sulfate isotopes, the isotopic composition could be calculated of the sulfate, which diffused downward across the 129 cm depth horizon. Although the isotopic composition of pore water sulfate at 129 cm depth was +43‰, the diffusive mass transfer of sulfate downward

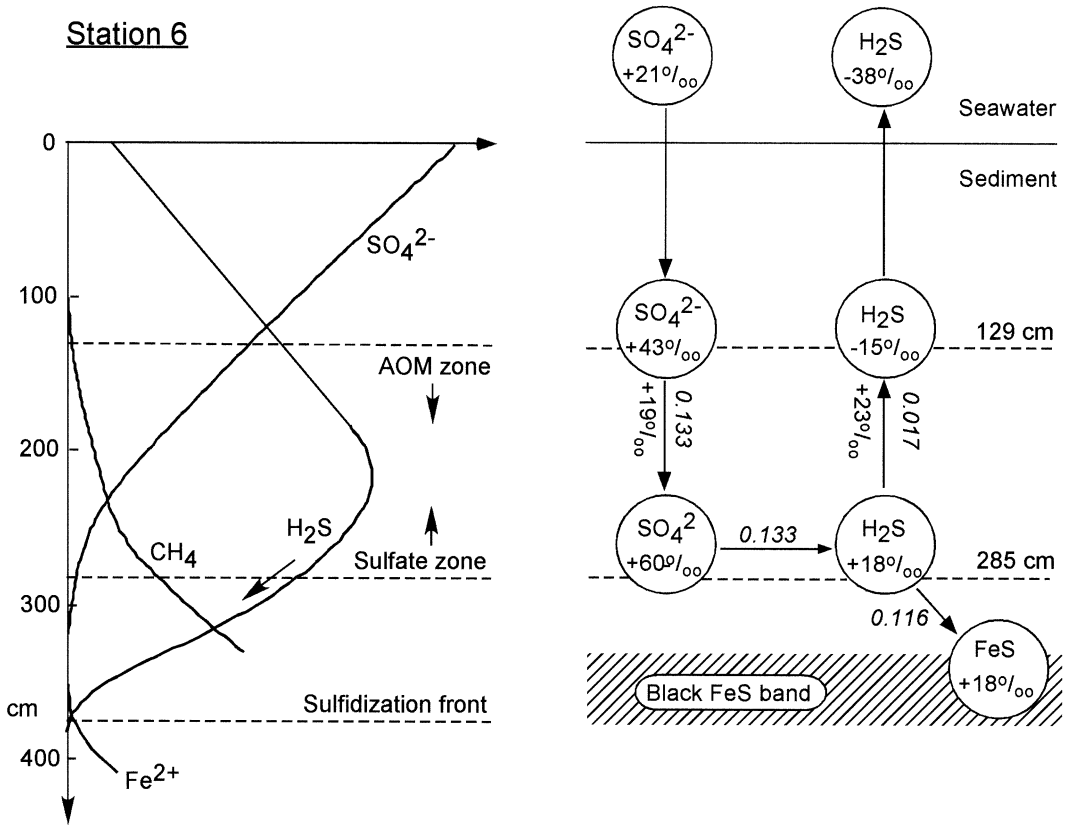

Fig. 11. Model of the sulfur cycle in Black Sea sediments showing the dual diffusion interfaces of sulfate–methane and sulfide–iron, based on data from Station 6. Left: Pore water gradients modeled from data in Figure 7 (the Fe^{2+} gradient is inferred from Stations 5 and 7). Right: Model of the sulfur mass balance and its isotopic composition as a function of reaction and diffusion. The model shows the SO_4^{2-} and H_2S pools at the sediment–water interface, at the 129 cm depth horizon where anaerobic oxidation of methane (AOM) starts, and at the H_2S peak within the SO_4^{2-}-CH_4 interface. H_2S diffuses downward from this H_2S peak to form a black FeS band (and subsequently FeS_2) at the sulfidization front in the underlying limnic sediment. Circles: Sulfur pools and their $\delta^{34}S$ values. Numbers on arrows: $\delta^{34}S$ of diffusion fluxes of SO_4^{2-} and H_2S. Italics: Sulfur fluxes in mmol m^{-2} d^{-1}. Notice that the downward diffusion flux of SO_4^{2-} is isotopically much lighter than the sulfate pool at the same depth. Correspondingly, the upward flux of H_2S is isotopically much heavier than the H_2S pool at the same depth. The isotopic mass balance of the two fluxes results in a net downward transport of sulfur with an isotopic composition of +18‰. Accordingly, this is the isotopic composition of H_2S at its peak concentration and of the FeS and FeS_2 formed by the progressing sulfidization of the limnic sediment.

across that same depth was isotopically much lighter, +19‰. This is due to the increase in $\delta^{34}SO_4^{2-}$ with depth, which implies that $^{32}SO_4^{2-}$ is depleted relatively faster with depth than $^{34}SO_4^{2-}$ and, thus, that $^{32}SO_4^{2-}$ has a relatively steeper gradient than $^{34}SO_4^{2-}$. Consequently, the sulfate diffusing downward is enriched in ^{32}S relative to the ambient sulfate pool in the pore water.

Such an effect of diffusion on the isotopic mass balance of sulfur in marine sediments was demonstrated for different marine sediments by Goldhaber and Kaplan (1980) and Chanton et al. (1987b). Based on their measured data, these authors also discussed the mechanisms and consequences of diffusion for the sulfur isotope geochemistry.

4.5.2. $\delta^{34}S$ of Diffusing Sulfide

Similar calculations were made for H_2S and its two isotopes, $H_2{}^{32}S$ and $H_2{}^{34}S$. From laboratory experiments it was found that the two sulfur isotopes in H_2S have diffusion coefficients that differ less than 1% at neutral pH (Piel, 1999), and the same D_s was therefore used for both. In this case, the H_2S decreased towards the sediment surface and the flux was accordingly directed upward. The increase in $\delta^{34}S$ of H_2S with depth (Fig. 7), combined with the increase in total H_2S concentration with depth, implies that the gradient of ^{34}S was relatively steeper than the gradient of ^{32}S. Consequently, the H_2S diffused upward across the 129 cm depth horizon with a much heavier isotopic composition, +23‰, than that of the pore water H_2S pool at the same depth, −15‰. It is remarkable that the upwards diffusing H_2S at 129 cm was isotopically 4‰ heavier than the downwards diffusing SO_4^{2-}, although the pore water H_2S at the same depth was 58‰ lighter than the SO_4^{2-}.

The upwards diffusing H_2S was 40–50‰ heavier than the H_2S present in the bottom water of the Black Sea. Although this H_2S flux does indeed contribute to the H_2S pool in the water column, and although the entire H_2S production in the sediment may be equally important as that in the water column on an

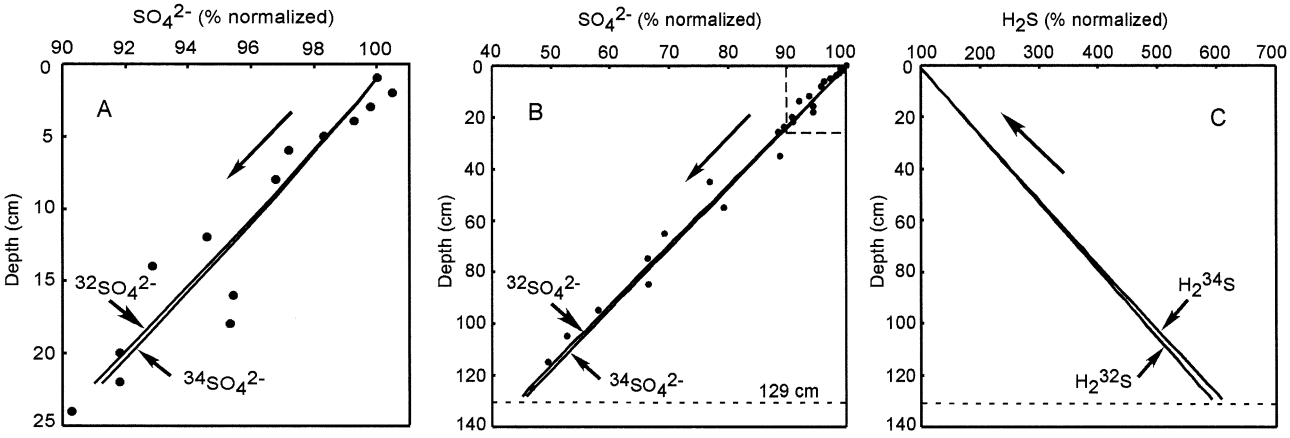

Fig. 12. (A and B) Sulfate concentrations measured in sediment pore water of Station 6 (●) compared to the gradients of $^{32}SO_4^{2-}$ and $^{34}SO_4^{2-}$ calculated from a linear regression of measured $\delta^{34}S$ values for SO_4^{2-} (data from Fig. 7). All data were normalized to 100% at the sediment surface. The two isotope gradients show the relatively steeper depletion of $^{32}SO_4^{2-}$ than of $^{34}SO_4^{2-}$, which is a consequence of the depth increase in the $\delta^{34}S$ of SO_4^{2-}. The narrow depth interval shown in frame A is indicated by broken lines in frame B. The broken line at 129 cm depth indicates the upper boundary of the zone of anaerobic methane oxidation. (C) The relative gradients of $H_2{}^{32}S$ and $H_2{}^{34}S$ are shown normalized to 100% at the sediment surface. The relatively steeper accumulation of $H_2{}^{34}S$ than of $H_2{}^{32}S$ with depth results in an enrichment in $H_2{}^{34}S$ in upwards diffusing sulfide relative to the ambient pore water sulfide.

areal basis (Weber et al., 2001), the large isotopic difference does not constitute a conflict. The upward H_2S flux from the zone of anaerobic methane oxidation was 0.017 mmol m^{-2} d^{-1} (Table 3 *(4)*) which is only 3% of the H_2S production from sulfate reduction in the uppermost 0–15 cm of the sediment (Jørgensen et al., 2001). Thus, 97% of the H_2S entering the water column is derived from the surface sediment and is isotopically light.

The deep, diffusive, methane-driven H_2S flux is consequently without significance for the total mass balance and isotopic composition of H_2S in the Black Sea water column.

4.5.3. The Isotope Effect of Diffusion

This isotopic difference between diffusing species and their pools at any depth may appear counter-intuitive, but it is critical for the sulfur isotopic mass balance of marine sediments. Figure 12 illustrates this important point which relates to all diffusing species that have a depth variation in isotopic composition. It should be noted that the mechanism is not related to a difference in diffusion coefficients of the two isotopes.

The sulfate gradients in the uppermost 25 cm of the sediment at Station 6 are shown in Figure 12A on a relative scale with all values at the sediment–water interface set at 100%. The measured sulfate data are here compared to the relative concentration gradients of ^{32}S and ^{34}S sulfate calculated from a linear regression of the $\delta^{34}S$ data for sulfate shown in Figure 7. Figure 12A shows that ^{32}S-sulfate has a relatively steeper gradient than ^{34}S-sulfate, although the difference is very small. This is a result of the increase in $\delta^{34}S$ of sulfate with depth which means that, although sulfate is overall being depleted at depth, the ^{34}S sulfate is not depleted quite as steeply as the ^{32}S-sulfate. Consequently, ^{32}S-sulfate must have a relatively higher downward diffusion flux than ^{34}S-sulfate and, thus, the total sulfate diffusing downward must be enriched in ^{32}S relative to the ambient pore water sulfate. Figure 12B shows the measured sulfate data and the modeled gradients of ^{32}S-sulfate and ^{34}S-sulfate down to the zone of anaerobic methane oxidation at 129 cm where the isotope flux of sulfate was calculated. Although the difference in gradients of the two isotopes is hardly visible on this scale, the actual minute difference has profound consequences for the isotopic mass balance.

By similar argumentation, sulfide diffusing upward must be enriched in ^{34}S relative to the ambient pore water sulfide. Figure 12C shows the relative concentration gradients of ^{32}S and ^{34}S-sulfide calculated from a linear regression of the $\delta^{34}S$ data for sulfide shown in Figure 7. Figure 12C shows that ^{34}S-sulfide has a relatively steeper gradient than ^{32}S-sulfide. This is a result of the increase in $\delta^{34}S$ of sulfide with depth. Consequently, the total upward flux of sulfide is enriched in ^{34}S relative to the ambient pore water sulfide.

The combined effects of differential isotope diffusion for sulfate and for sulfide is A) to dampen the increase in $\delta^{34}S$ of sulfate with depth relative to the increase that would have occurred without such a differential diffusion, and B) to retain lighter sulfide at depth by preferentially expelling the heavier sulfide. The net result is that the sulfide pool at depth may approach an isotopic composition close to that of seawater sulfate. This deceivingly mimics the result of closed system diagenesis although the mechanism is based on an open diffusional system.

4.5.4. Isotope Mass Balance

From the isotopic difference between the downward SO_4^{2-} flux and the upward H_2S flux, an isotope mass balance can now be calculated for the net sulfur flux across the 129 cm depth horizon (Fig. 11). The net downward flux should at steady state correspond to the total amount of sulfur which is currently being immobilized as AVS, FeS_2, and organic sulfur below that depth. This net flux was (0.133–0.017=) 0.116 mmol S m^{-2} d^{-1} and it had a net isotopic composition of +18‰. Thus, the

upward diffusion of heavy H_2S reduced slightly the $\delta^{34}S$ of the sulfur brought down by diffusion of light sulfate.

The downward net flux of sulfur and its isotopes must be identical to the accumulation rate of sulfur and to its isotopic composition. This was also the case. The FeS_2, which comprises the bulk of immobilized sulfur in the sediment below 129 cm depth, had an isotopic composition of +16 to +19‰. This corresponds closely to the +18‰ calculated for the net flux of pore water sulfur and confirms the isotopic mass balance model.

The FeS_2 apparently accumulates the history of iron–sulfur precipitation which starts with AVS at the black band and gradually converts into pyrite above the black band as the H_2S front moves downward. The AVS within that interval was lighter in the upper part where it was precipitated from a lighter pore water H_2S pool (Fig. 7). Within the black band of AVS at the lower diffusion front of H_2S around 300 cm depth, the AVS had a $\delta^{34}S$ of +16‰. This is close to both the net flux of sulfur isotopes and to the isotopic composition, +18‰, of H_2S just above the black band.

In conclusion, the accumulation of isotopically very heavy sulfide in the Black Sea sediments is due to the immobilization of heavy H_2S formed from methane-driven sulfate reduction. The fractionation and diffusion mechanisms described here are active in all marine sediments but they reach their extremes under the special conditions available in the Black Sea. These sediments are extraordinary in that the underlying limnic horizons have a large excess of reactive iron which draws down efficiently the H_2S formed at the sulfate–methane interface. Because the limnic sediment intrinsically had only a low FeS and FeS_2 content, the large amounts of iron sulfide species formed today at the sulfidization front totally dominate and overprint the isotopic signal of the limnic sulfur minerals. In most other marine sediments, the heavy isotopic signal of deep pyrite formation is swamped by the large pool of isotopically light pyrite which was originally formed nearer to the sediment surface.

At all four stations, the sulfur immobilized as pyrite below the H_2S peak reached $\delta^{34}S$ values of +15‰ to +30‰, thus indicating that similar mechanisms were involved in the isotopic net fluxes. It is an interesting observation that this deep and heavy H_2S may occasionally appear up at the sediment surface in areas where deep pore water is transported up by advection in methane seeps. Such seeps are abundant on the outer shelf and upper slope of the northwestern Black Sea, and carbonate structures form on the sea bed around these seeps by anaerobic oxidation of methane, even below the chemocline depth (Ivanov et al., 1998; Luth et al., 1999; Michaelis et al., 2002). Pyrite enclosed in the carbonate has been found to have isotopically very heavy sulfur (Peckmann et al., 2001). However, the origin of the pyrite is not yet clear.

4.5.5. Deep Sulfide Sinks in Marine Sediments

The deep sink for methane-derived H_2S may be extreme in the Black Sea, but it is not unique. A downwards progressing sulfidization front has also been found below Holocene sediments in the Baltic Sea (Boesen and Postma, 1988), in Kau Bay (Middelburg, 1991), and below sapropels in the eastern Mediterranean (Passier et al., 1996). A SO_4^{2-}-CH_4 interface with enhanced H_2S production is generally found in shelf and slope sediments and also in many deep-sea sediments (Borowski et al., 1999). We are not aware of published observations on an H_2S-Fe^{2+} interface based on direct pore water analyses in marine sediment cores. However, this may be due to its occurrence deep within the zone of methane supersaturation which complicates the analysis of rapidly oxidizable Fe^{2+}.

Evidence for a draw-down of sulfide is found also in many other sedimentary provinces of the world ocean, although mostly less distinct. What are the signals of a deep sink for methane-derived H_2S? 1) A decrease of H_2S below its maximum at the SO_4^{2-}-CH_4 interface. This decrease is often observed (Goldhaber and Kaplan, 1974, 1980; Schulz et al., 1994; Pruysers, 1998; Fossing et al., 2000), yet data are often only available to see the beginning of the decrease. 2) The occurrence of a distinct zone of Fe and S-accumulation and/or a peak of magnetic susceptibility at some depth below the SO_4^{2-}-CH_4 interface. Such a zone or peak has indeed been observed in several deep sea sediment cores, e.g., from the South Atlantic (Niewöhner et al., 1998; Kasten et al., 1998). 3) The mass balance of sulfur fluxes modeled for different ocean margin sediments which shows that the SO_4^{2-} flux into the sediment minus the H_2S flux out of the sediment often exceeds the net immobilization of sulfur within the sulfate zone (B. B. Jørgensen, unpublished data). An additional sulfide sink seems to be required to account for the excess sulfur influx through the pore water. We suggest that this sink is the deeply mobilized iron and that the draw-down of sulfide occurs much more widely than previously recognized. 4) The formation of ^{34}S-enriched pyrite. Separate isotope analyses of individual pyrite crystals may make it possible to discriminate pyrite formed early upon burial or deeply from methane-derived H_2S formation.

4.5.6. Open or Closed System Diagenesis

The formation of isotopically heavy pyrite observed here is not the result of closed system diagenesis in the classical sense. A sediment functions as a closed system if there is limited diffusional exchange to the overlying seawater during diagenesis. The remaining sulfate pool and the sulfide concurrently produced become progressively enriched in ^{34}S as ^{32}S is preferentially removed from the dwindling sulfate pool (Rayleigh-type fractionation). Ultimately, the accumulated sulfides in a completely closed system will reach the same sulfur isotopic composition as seawater sulfate, ca. +20‰, due to conservation of mass for both ^{32}S and ^{34}S when all sulfate has been reduced. As discussed above, the Black Sea sediments are as open to diffusional exchange with the overlying seawater as are most other modern sediments.

In our opinion, the classical discussion of closed vs. open system diagenesis, when used to interpret sulfur isotopic compositions in ocean margin sediments, has been misleading. The reason for this is that the interpretation does not take into account that the vertical diffusion fluxes of SO_4^{2-} and H_2S have isotopic compositions completely different from those which are measured in the pore water pools of SO_4^{2-} and H_2S. When SO_4^{2-} and H_2S become isotopically heavier with depth, it is not because of a transition to more closed system diagenesis. Exactly the same will happen in a system that is completely open, i.e., a system where practically all the sulfate diffusing down comes back up as H_2S and where there is insignificant retention

of sulfur by pyrite formation. Jørgensen (1979) made a model calculation of such a situation, assuming an isotopic fractionation of 50‰ during sulfate reduction and 90% of the H_2S returning to the sediment surface. The model showed that, although the $\delta^{34}S$ at the sediment surface was +20‰ for SO_4^{2-} and –17‰ for H_2S, the SO_4^{2-} would diffuse downward across the sediment–water interface with an isotopic composition of –17‰ whereas the H_2S would diffuse upward with a similar isotopic composition of –17‰.

Based on concentration and isotope data for sulfur species in sediments of the Gulf of California, Goldhaber and Kaplan (1980) calculated that sulfate diffused downward with an isotopic composition of −4.5‰. Importantly, those authors also showed that the isotopic fractionation factor, α, calculated for sulfate reduction in the sediment was much higher when assuming open system conditions ($\alpha = 1.060$) than when closed system conditions were assumed ($\alpha = 1.035$). The open system diagenesis was confirmed by the sulfur isotopic composition of metastable iron sulfide, an equivalent to the deep sink of amorphous sulfide in the Black Sea sediments. In a rapidly accumulating coastal sediment, Cape Lookout Bight, in which 77% of the sulfide produced from sulfate reduction was trapped within the sediment, Chanton et al. (1987a, b) found that H_2S diffusing up to the sediment surface was highly enriched in ^{34}S ($\delta^{34}S = +15.9‰$) relative to the sulfide produced in the surface sediment. Thus, even in this sediment which would be considered predominantly closed with respect to sulfide, the isotope effect of diffusion was very significant.

5. CONCLUSIONS

The $\delta^{34}S$ of sedimentary pyrite depends primarily on, at which relative depth within the SO_4^{2-}-H_2S gradients it is formed (relative depth being defined by the fraction of sulfate remaining). The deeper it forms, the more ^{34}S-enriched is the SO_4^{2-} and, therefore, also the H_2S from which the pyrite precipitates. Due to the increase in $\delta^{34}S$ of SO_4^{2-} and H_2S with depth, the heaviest sulfide is found at the bottom of the sulfate zone, which is right at the sulfate–methane transition. Because sulfate reduction rates are particularly high at that transition, the production rates of isotopically heavy H_2S also are particularly high. It may appear as a paradox that the sulfate reduction is most intensive where the sulfate concentration approaches zero and has its most extreme isotopic composition.

What is so special about the Black Sea sediments is that exactly this sulfide becomes efficiently trapped by diffusion downward to the diagenetic front in the limnic zone where it constitutes the main sulfur pool and therefore determines the overall $\delta^{34}S$ value of amorphous iron sulfide, greigite, and pyrite. The amount of sulfide trapped down there corresponds to only a minute fraction, 1.9–4.3%, of the overall sulfate reduction in the whole sediment column (Table 3, *(8)*). It is, however, a large fraction, 19–50%, of the sulfate reduction in the sulfate–methane transition (Table 3, *(10)*).

The formation of isotopically heavy pyrite in the Pleistocene deposits, with $\delta^{34}S$ values of up to +30‰, was observed at all stations, from the shelf break above the chemocline to the sulfidic deep sea. This shows that the deep formation of isotopically heavy pyrite is independent of the oxygen or sulfide history of the water column. It also shows that the highly ^{34}S-enriched pyrite did not originate from pyrite formed in the water column but that it is a product of the progressing sulfidization of limnic iron-rich sediment due to methane-driven production of isotopically heavy H_2S.

In contrast, pyrite in the Black Sea surface deposits was most ^{34}S-depleted at the deep stations underlying the sulfidic water column where it probably originated mostly from syngenetic pyrite formed near the chemocline and sedimenting into the anoxic deep sea. At all stations, the diffusion flux of H_2S across the sediment–water interface was directed upward, irrespective of the H_2S concentration in the water column. Consequently, diagenetic pyrite formation throughout the three units was based on H_2S produced within the sea bed and not on H_2S from the water column.

There is a complication to this argument with respect to the sulfur isotopes, however. Because the ratio between the diffusion gradients of $H_2{}^{32}S$ and $H_2{}^{34}S$ is dependent on the $\delta^{34}S$ of H_2S in the water column, the resulting $\delta^{34}S$ of H_2S within the sediment (and thus of the pyrite formed from this H_2S) also is coupled to the $\delta^{34}S$ of H_2S in the water column. The residence time of H_2S in the Black Sea water column is estimated at 90–150 yr (Neretin et al., 2001) or longer. The diffusion time of H_2S from the sulfate–methane transition and up to the sediment surface is 2–3 times longer, ca. 300 yr (560 yr for sulfate times the ratio of diffusion coefficients, $D(SO_4^{2-})/D(H_2S)$). In our isotope flux calculations in Section 4.5. we have tacitly assumed that the $\delta^{34}S$ of SO_4^{2-} and H_2S in the water column have remained in quasi-steady-state for many hundreds of years.

It is apparent from the present results that the isotopic mass balance of the sediment and the formation of light or heavy pyrite cannot be explained simply from the classical terms of open vs. closed system diagenesis. On the contrary, these terms are confusing because all modern marine sediments are basically very open systems and because the concepts do not take into account the isotope effect of diffusion. It is the differential diffusion fluxes of the two sulfur isotopes in SO_4^{2-} or H_2S which may lead to false interpretations of the isotopic signals in sediment sulfides. The downward diffusion of sulfate tends to reduce the effect of isotope fractionation during sulfate reduction by preferentially delivering the lighter isotope. Similarly, the upward diffusion of sulfide preferentially removes the heavy isotope and brings it back to the sediment surface. The net result is the formation at depth of pyrite with an isotopic composition close to that of seawater sulfate. This may be a similar result as would have been reached by closed system diagenesis, but for very different reasons.

High positive $\delta^{34}S$ values of pyrite, as seen in the Black Sea sediments, are found also in many sedimentary rocks formed throughout the last 2–3 billion years of earth's history (Canfield and Raiswell, 1999). There may be several possible causes for such high $\delta^{34}S$ values. The present study shows one mechanism by which open system diagenesis with extensive diffusion exchange to the overlying seawater may lead to isotopically heavy sedimentary sulfides. The special conditions prevailing in formerly limnic marginal seas specifically trap heavy sulfides. The key mechanism is a combination of methane-driven sulfate reduction and a deep H_2S trap. The double diffusion fronts of SO_4^{2-}-CH_4 and H_2S-Fe^{2+} found in Black Sea sediments are indicators of such a mechanism.

Acknowledgments—We thank Alexander Kohly for information on the stratification of fossil diatoms and Kathrina Hilgenfeldt and Ulrich Bleil for the permission to quote their magnetic susceptibility data. Alexander Rozanov, Kirsten Habicht, Bo Thamdrup, and Tim Ferdelman contributed with helpful discussions. Andreas Weber, Christoph Hempel, and the crew and captain of *R/V Petr Kottsov* are thanked for all their efforts to make the cruise successful. We thank our excellent teams of sediment coring, Dan Secrieru, Volker Meyer, and Ulf Luth and of laboratory analytics, Kirsten Neumann and Swantje Fleischer for enjoyable collaboration. Jürgen Rullkötter and Hans Brumsack are thanked for access to analytical facilities of the ICBM, University of Oldenburg. We thank Martin B. Goldhaber and two anonymous reviewers for constructive and helpful reviews of the manuscript. This study was financially supported by the German Max Planck Society, the Deutsche Forschungsgemeinschaft, and the Fonds der Chemischen Industrie.

Associate editor: D. E. Canfield

REFERENCES

Aksu A. E., Hiscot R. N., and Yaşar D. (1999) Oscillating Quaternary water levels of the Marmara Sea and vigorous outflow into the Aegean Sea from the Marmara Sea –Black Sea drainage corridor. *Mar. Geol.* **153,** 275–302.

Albert D. B., Taylor C., and Martens C. S. (1995) Sulfate reduction rates and low molecular weight fatty acid concentrations in the water column and surficial sediments of the Black Sea. *Deep-Sea Res.* **42,** 1239–1260.

Arthur M. A. and Dean W. E. (1998) Organic-matter production and preservation and evolution of anoxia in the Holocene Black Sea. *Paleoceanography* **13,** 395–411.

Beaudoin G., Taylor B. E., Rumble D., III, and Thiemens M. (1994) Variations in the sulfur isotope composition of troilite from the Cañon Diablo iron meteorite. *Geochim. Cosmochim. Acta* **58,** 4253–4255.

Berg P., Risgaard-Petersen N., and Rysgaard S. (1998) Interpretation of measured concentration profiles in sediment pore water. *Limnol. Oceanogr.* **43,** 1500–1510.

Berner R. A. (1969) Migration of iron and sulfur within anaerobic sediments during early diagenesis. *Am. J. Sci.* **267,** 19–42.

Berner R. A. (1974) Iron sulfides in Pleistocene deep Black Sea sediments and their paleo-oceanographic significance. In *The Black Sea—Geology, Chemistry, Biology* (eds. E. T. Degens and D. A. Ross), pp. 524–531. Plenum Press.

Boesen C. and Postma D. (1988) Pyrite formation in anoxic environments of the Baltic. *Am. J. Sci.* **288,** 575–603.

Bolliger C., Schroth M. H., Bernasconi S. M., Kleikemper J., and Zeyer J. (2001) Sulfur isotope fractionation during microbial sulfate reduction by toluene-degrading bacteria. *Geochim. Cosmochim. Acta* **65,** 3289–3298.

Bonev I. K., Khrischev Kh. G., Neikov H. N., and Georgiev V. M. (1989) Mackinawite and greigite in iron sulphide concretions from Black Sea sediments. *Comptes rendus de l'Académie bulgare des Sciences* **42,** 97–100.

Borowski W. S., Paull C. K., and Ussler W., III.. (1999) Global and local variations of interstitial sulfate gradients in deep-water, continental margin sediments: Sensitivity to underlying methane and gas hydrates. *Mar. Geology* **159,** 131–154.

Böttcher M. E. and Lepland A. (2000) Biogeochemistry of sulfur in a sediment core from the west-central Baltic Sea: Evidence from stable isotopes and pyrite textures. *J. Mar. Syst.* **25,** 299–312.

Böttcher M. E., Thamdrup B., and Vennemann T. W. (2001) Oxygen and sulfur isotope fractionation during anaerobic bacterial disproportionation of elemental sulfur. *Geochim. Cosmochim. Acta* **65,** 1601–1609.

Böttcher M. E., Schale H., Schnetger B., Wallmann K., and Brumsack H. J. (2000) Stable sulfur isotopes indicate net sulfate reduction in near-surface sediments of the deep Arabian Sea. *Deep-Sea Res. II* **47,** 2769–2783.

Böttcher M. E., Khim B.-K., Suzuki A., Gehre M., Wortmann U. and Brumsack H.-J. Microbial sulfate reduction in deep sediments of the southwest Pacific(ODP Leg 181, Sites 1119 to 1125): Evidence from stable sulfur sulfur isotope fractionation and pore water modeling. *Mar. Geol.* (in press).

Brumsack H. J. (1989) Geochemistry of recent TOC-rich sediments from the Gulf of California and the Black Sea. *Geologische Rundschau* **78,** 851–882.

Bukry D. (1974) Coccoliths as paleosalinity indicators—Evidence from the Black Sea. In *The Black Sea—Geology, Chemistry, Biology* (eds. E. T. Degens and D. A. Ross), pp. 353–363. Plenum Press.

Calvert S. E. and Fontugne M. (1987) Stable carbon isotope evidence for the marine origin of the organic matter in the Holocene Black Sea sapropel. *Chem. Geol.* **66,** 315–322.

Calvert S. E. and Karlin R. E. (1998) Organic carbon accumulation in the Holocene sapropel of the Black Sea. *Geology* **26,** 107–110.

Calvert S. E., Vogel J. S., and Southon J. R. (1987) Carbon accumulation rates and the origin of the Holocene sapropel in the Black Sea. *Geology* **151,** 918–921.

Calvert S. E., Thode H. G., Yeung D., and Karlin R. E. (1996) A stable isotope study of pyrite formation in the Late Pleistocene and Holocene sediments of the Black Sea. *Geochim. Cosmochim. Acta* **60,** 1261–1270.

Canfield D. E. (2001) Isotope fractionation by natural populations of sulfate-reducing bacteria. *Geochim. Cosmochim. Acta* **65,** 1117–1124.

Canfield D. E. and Raiswell R. (1999) The evolution of the sulfur cycle. *Am. J. Sci.* **299,** 697–723.

Canfield D. E. and Thamdrup B. (1994) The production of ^{34}S-depleted sulfide during bacterial disproportionation of elemental sulfur. *Science* **266,** 1973–1975.

Canfield D. E., Lyons T. W., and Raiswell R. (1996) A model for iron deposition to euxinic Black Sea sediments. *Am. J. Sci.* **296,** 818–834.

Chanton J. P., Martens C. S., and Goldhaber M. B. (1987a) Biogeochemical cycling in an organic-rich coastal marine basin. 7. Sulfur mass balance, oxygen uptake and sulfide retention. *Geochim. Cosmochim. Acta* **51,** 1187–1199.

Chanton J. P., Martens C. S., and Goldhaber M. B. (1987b) Biogeochemical cycling in an organic-rich coastal marine basin. 8. A sulfur isotopic budget balanced by differential diffusion across the sediment-water interface. *Geochim. Cosmochim. Acta* **51,** 1201–1208.

Cline J. D. (1969) Spectrophotometric determination of hydrogen sulfide in natural waters. *Limnol. Oceanogr.* **14,** 454–458.

Cornwell J. C. and Morse J. W. (1987) The characterization of iron sulfide minerals in anoxic marine sediments. *Mar. Chem.* **22,** 193–206.

Cypionka H., Smock A. M., and Boettcher M. E. (1998) A combined pathway of sulfur compound disproportionation in *Desulfovibrio desulfuricans*. *FEMS Microbiol. Lett.* **166,** 181–186.

Egorov A. V. (2000) Methane biogeochemistry in the sediments of the Baltic and Black Seas: Kinetic models of diagenesis. *Oceanology* **40,** 647–653.

Fossing H. and Jørgensen B. B. (1989) Measurement of bacterial sulfate reduction in sediments. Evaluation of a single-step chromium reduction method. *Biogeochemistry* **8,** 205–222.

Fossing H., Ferdelman T. G., and Berg P. (2000) Sulfate reduction and methane oxidation in continental margin sediments influenced by irrigation (South-East Atlantic off Namibia). *Geochim. Cosmochim. Acta* **64,** 897–910.

Fry J., Jannasch H. W., Molyneaux S. J., Wirsen C. O., Muramoto J. A., and King S. (1991) Stable isotope studies of the carbon, nitrogen and sulfur cycles in the Black Sea and the Cariaco Trench. *Deep-Sea Res.* **38,** S1003–S1019.

Goldhaber M. B. and Kaplan I. R. (1974) Controls and consequences of sulfate reduction rates in recent marine sediments. *Soil Sci.* **119,** 42–55.

Goldhaber M. B. and Kaplan I. R. (1980) Mechanisms of sulfur incorporation and isotope fractionation during early diagenesis in sediments of the Gulf of California. *Mar. Chem.* **9,** 95–143.

Görür N., Çağgatay M. N., Emre Ö., Bedri A., Sakinç M., İslamoğglu Y., Algan O., Erkal T., Keçer M., Akkök R., and Karlik G. (2001) Is the abrupt drowning of the Black Sea shelf at 7150 yr BP a myth? *Mar. Geol.* **176,** 65–73.

Habicht K. S. and Canfield D. E. (2001) Isotope fractionation by sulfate-reducing natural populations and the isotopic composition of sulfide in marine sediments. *Geology* **29,** 555–558.

Habicht K. S., Canfield D. E., and Rethmeier J. (1998) Sulfur isotope fractionation during bacterial reduction and disproportionation of thiosulfate and sulfite. *Geochim. Cosmochim. Acta* **62,** 2585–2595.

Hay B. J. (1988) Sediment accumulation in the central western Black Sea over the past 5100 years. *Paleoceanography* **3,** 491–508.

Hay B. J., Arthur M. A., Dean W. E., Neff E. D., and Honjo S. (1991) Sediment deposition in the Late Holocene abyssal Black Sea with climatic and chronological implications. *Deep-Sea Res.* **38 (***Suppl. 2***),** S1211–S1235.

Ivanov M. K., Limonov A. F., and Woodside J. M. (1998) Extensive deep fluid flux through the sea floor on the Crimean continental margin (Black Sea). In *Gas Hydrates: Relevance to World Margin Stability and Climate Change* (eds. J.-P. Henriet and J. Mienert), pp. 196–213. Geol. Soc. London, Spec. Publ. 137.

Iversen N. and Jørgensen B. B. (1993) Diffusion coefficients of sulfate and methane in marine sediments: Influence of porosity. *Geochim. Cosmochim. Acta* **57,** 571–578.

Jones G. A. and Gagnon A. R. (1994) Radiocarbon chronology of Black Sea sediments. *Deep-Sea Res.* **41,** 531–557.

Jørgensen B. B. (1979) A theoretical model of the stable sulfur isotope distribution in marine sediments. *Geochim. Cosmochim. Acta* **43,** 363–374.

Jørgensen B. B. (1990) A thiosulfate shunt in the sulfur cycle of marine sediments. *Science* **249,** 152–154.

Jørgensen B. B., Bang M., and Blackburn T. H. (1990) Anaerobic mineralization in marine sediments from the Baltic Sea-North Sea transition. *Mar. Ecol. Prog. Ser.* **59,** 39–54.

Jørgensen B. B., Weber A., and Zopfi J. (2001) Sulfate reduction and anaerobic methane oxidation in Black Sea sediments. *Deep-Sea Res.* **48,** 2097–2120.

Kasten S., Freudenthal T., Gingele F. X., and Schulz H. D. (1998) Simultaneous formation of iron-rich layers at different redox boundaries in sediments of the Amazon deep-sea fan. *Geochim. Cosmochim. Acta* **62,** 2253–2264.

Lein A.Yu. and Ivanov M. V. (1991) On the sulfur and carbon balances in the Black Sea. In *Black Sea Oceanography* **351** (eds. E. Izdar and J. W. Murray), pp. 307–318. NATO ASI Series, Kluwer.

Lie L. (1994) Sulfur species and their isotope composition in Caucasus shelf and continental slope sediments. Ph.D. thesis, Institute of Oceanology, Russian Academy of Sciences, Moscow. 104 pp.

Lüschen H. (1998) High-resolution geochemical analysis of a sediment core from the Black Sea. M.Sc. thesis, University of Oldenburg, Germany. 134 pp.

Luth C., Luth U., Gebruk A. V., and Thiel H. (1999) Methane gas seeps along the oxic/anoxic gradient in the Black Sea: Manifestations, biogenic sediment compounds, and preliminary results on benthic ecology. *P. S. Z. N. Mar. Ecol.* **20,** 221–249.

Luther G. W., III. (1991) Pyrite synthesis via polysulfide compounds. *Geochim. Cosmochim. Acta* **55,** 2839–2849.

Lyons T. W. (1991) Upper Holocene sediments of the Black Sea: Summary of leg 4 box cores (1988 Black Sea oceanographic expedition). In *Black Sea Oceanography* (eds. E. Izdar and J. W. Murray), pp. 401–441. NATO ASI Series, Kluwer.

Lyons T. W. (1997) Sulfur isotopic trends and pathways of iron sulfide formation in upper Holocene sediments of the anoxic Black Sea. *Geochim. Cosmochim. Acta* **61,** 3367–3382.

Michaelis W., Seifert R., Nauhaus K., Treude T., Thiel V., Blumenberg M., Knittel K., Gieseke A., Peterknecht K., Pape T., Boetius A., Amann R., Jørgensen B. B., Widdel F., Peckmann J., Pimenov N. V., and Gulin M. B. (2002) Microbial reefs in the Black Sea fuelled by anaerobic oxidation of methane. *Science* **297,** 1013–1015.

Middelburg J. J. (1991) Organic carbon, sulphur, and iron in recent semi-euxinic sediments of Kau Basin, Indonesia. *Geochim. Cosmochim. Acta* **55,** 825–828.

Müller G. and Stoffers P. (1974) Mineralogy and petrology of Black Sea basin sediments. In *The Black Sea–Geology, Chemistry and Biology* (eds. E. T. Degens and D. A. Ross), pp. 265–296. Plenum Press.

Muramoto J. A., Honjo S., Fry B., Hay B. J., Howarth R. W., and Cisne J. L. (1991) Sulfur, iron and organic carbon fluxes in the Black Sea: Sulfur isotopic evidence for origin of sulfur fluxes. *Deep-Sea Res.* **38 (***Suppl. 2***),** S1151–S1187.

Murray J. W., Top Z., and Özsoy E. (1991) Hydrographic properties and ventilation of the Black Sea. *Deep-Sea Res.* **38 (***Suppl. 2***),** S663–S689.

Neretin L. N., Böttcher M. E., and Volkov I. I. (1998a) The stable isotopic composition of sulfur species in the Black Sea water column. *Mineral. Mag.* **62A,** 1075–1076.

Neretin L., Böttcher M. E., Jørgensen B. B., Volkov I. I., and Lüschen H. (1998b) Pyritization at the Holocene/Late Pleistocene transition in the Black Sea sediments: Sulfur species and their isotopic composition. In *Geochemistry of the Earth's Surface* (ed. H. Armannsson), pp. 331–334. A. A. Balkema, Rotterdam.

Neretin L. N., Volkov I. I., Böttcher M. E., and Grinenko V. A. (2001) A sulfur budget for the Black Sea anoxic zone. *Deep-Sea Res. I* **48,** 2569–2593.

Neretin L. N., Böttcher M. E., Jørgensen B. B., Volkov I. I., Lüschen H. and Hilgenfeldt K. (2004) Pyritization in the upper Pleistocene sediments of the Black Sea driven by anaerobic methane oxidation. *Geochim. Cosmochim. Acta* **68**(9), 2081–2093.

Nicolaev S. D. (1995) *Isotope Paleoceanography of Continental Seas*126 pp. VNIRO, Moscow.

Niewöhner C., Hensen C., Kasten S., Zabel M., and Schulz H. D. (1998) Deep sulfate reduction completely mediated by anaerobic methane oxidation in sediments of the upwelling area off Namibia. *Geochim. Cosmochim. Acta* **62,** 455–464.

Nriagu J. O. and Soon Y. K. (1985) Distribution and isotopic composition of sulfur in lake sediments of northern Ontario. *Geochim. Cosmochim. Acta* **49,** 823–834.

Passier H. F., Middelburg J. J., de Lange G. J., and Böttcher M. E. (1999) Modes of sapropel formation in the eastern Mediterranean: Some constraints based on pyrite properties. *Mar. Geol.* **153,** 199–219.

Passier H. F., Middelburg J. J., van Os B. J. H., and de Lange G. J. (1996) Diagenetic pyritisation under eastern Mediterranean sapropels caused by downward sulphide diffusion. *Geochim. Cosmochim. Acta* **60,** 751–763.

Peckmann J., Reimer A., Luth U., Luth C., Hansen B. T., Heinicke C., Hoefs J., and Reitner J. (2001) Methane-derived carbonates and authigenic pyrite from the northwestern Black Sea. *Mar. Geol.* **177,** 129–150.

Piel C. (1999) Experimental studies of sulfur isotope fractionation ($^{34}S/^{32}S$) during transport and reaction of dissolved and gaseous sulfur species (in German). M.Sc. thesis, Univ. Bremen, Germany. 98 pp.

Pruysers P. A. (1998) Early diagenetic processes in sediments of the Angola Basin, eastern South Atlantic. Ph.D. thesis, University of Utrecht, The Netherlands. 135 pp.

Rickard D. and Luther G. W., III. (1997) Kinetics of pyrite formation by the H_2S oxidation of iron (II) monosulfide in aqueous solutions between 25 and 125 degrees Celsius: The mechanism. *Geochim. Cosmochim. Acta* **61,** 135–147.

Roselló-Mora R., Thamdrup B., Schäfer H., Weller R., and Amann R. (1999) The response of the microbial community of marine sediments to organic carbon input under anaerobic conditions. *System. Appl. Microbiol.* **22,** 237–248.

Ross D. A. and Degens E. T. (1974) Recent sediments of the Black Sea. In *The Black Sea—Geology, Chemistry and Biology* (eds. E. T. Degens and D. A. Ross), Am. Assoc. Petrol. Geol. Mem. 20, 183–199.

Ryan W. B. F., Pitman W. C., III, Major C. O., Shimkus K., Moskalenko V., Jones J. A., Dimitrov P., Gorur N., Sakinç M., and Yuce H. (1997) An abrupt drowning of the Black Sea shelf. *Mar. Geol.* **138,** 119–126.

Schulz H. D. (2000) Quantification of early diagenesis: Dissolved constituents in marine pore water. In *Marine Geochemistry* (eds. H. D. Schulz and M. Zabel), pp. 87–128. Springer.

Schulz H. D., Dahmke A., Schinzel U., Wallmann K., and Zabel M. (1994) Early diagenetic processes, fluxes, and reaction rates in sediments of the south Atlantic. *Geochim. Cosmochim. Acta* **58,** 2041–2060.

Skopintsev B. A. (1975) *Formation of the Contemporary Chemical Composition of the Black Sea*336 pp. Gidrometaoizdat, Leningrad.

Sokolov V. S (1980) The determination of reactive forms of Fe and Mn in marine sediments. In *Chemical Analysis of Marine Sediments* (in Russian), pp. 28–41. Nauka, Moscow.

Sten-Knudsen O. (1995) *Material Transport, Membrane Potentials, and Electrical Impulses Over Biological Membranes* (in Danish)526 pp. Akademisk Forlag, Copenhagen.

Thamdrup B., Roselló-Móra R., and Amann R. (2000) Microbial manganese and sulfate reduction in Black Sea shelf sediments. *Appl. Environ. Microbiol.* **66,** 2888–2897.

Vinogradov A. P., Grinenko V. A., and Ustinov V. I. (1962) Isotopic composition of sulphur compounds in the Black Sea. *Geokhimia* **10,** 973–997.

Volkov I. I. (1961) Ferrous iron sulfides: Their relationship and diagenesis in the Black Sea sediments (in Russian). *Trudy Instituta Okeanologii* **50,** 68–91.

Volkov I. I. (1973) Main features of the vertical distribution of chemical elements in deep-sea Black Sea sediments. *Lithology and Mineral Deposits* **2,** 3–22.

Volkov I. I. (1984) *Sulfur Geochemistry of Ocean Sediments* (in Russian)272 pp. Nauka, Moscow.

Volkov I. I and Zhabina N. N (1980) Method of determination of sulfur species in marine sediments. In *Chemical Analysis of Marine Sediments*, pp. 5–27. Nauka, Moscow.

Wang Q. and Morse J. W. (1996) Pyrite formation under conditions approximating those in anoxic sediments. I. Pathway and morphology. *Mar. Chem.* **52,** 99–121.

Weber A., Riess W., Wenzhoefer F., and Jørgensen B. B. (2001) Sulfate reduction in Black Sea sediments: *In situ* and laboratory radiotracer measurements from the shelf to 2000 m depth. *Deep-Sea Res. I* **48,** 2073–2096.

Wenzhöfer F., Riess W., and Luth U. (2002) *In situ* macrofaunal respiration rates and their importance for benthic carbon mineralization on the northwestern Black Sea shelf. *Ophelia* **56,** 87–100.

Wilkin R. T. and Arthur M. A. (2001) Variations in pyrite texture, sulfur isotope composition, and iron systematics in the Black Sea: Evidence for Late Pleistocene to Holocene excursions of the O_2-H_2S redox transition. *Geochim. Cosmochim. Acta* **65,** 1399–1416.

Wilkin R. T., Arthur M. A., and Dean W. E. (1997) History of water-column anoxia in the Black Sea indicated by pyrite framboid size distributions. *Earth Planet. Sci. Lett.* **148,** 517–525.

Zhabina N. N. and Volkov I. I. (1978) A method of determination of various sulfur compounds in sea sediments and rocks. In *Environmental Biochemistry and Geomicrobiology. Vol. 3. Methods, Metals, and Assessment* (ed. W. E. Krumbein), pp. 735–746. Ann Arbor Science.